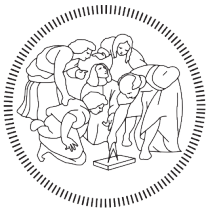

POLITECNICO
MILANO 1863

Final Report Group 11

Person code	*Surname*	*Name*
	Email	
10700183	Carlà	Giulio
	giulio.carla@mail.polimi.it	
10567508	Castelanelli Oddo	Alessandro
	alessandro.castelanelli@mail.polimi.it	
10908586	Papi	Jacopo
	jacopo.papi@mail.polimi.it	
10701291	Sapuppo	Andrea
	andrea1.sapuppo@mail.polimi.it	
10934963	Spinelli	Francesco
	francesco4.spinelli@mail.polimi.it	
10668572	Castoldi	Paolo
	paolo.castoldi@mail.polimi.it	

Course of Space system engineering and operations
School of Industrial Engineering
Academic Year 2022-2023

Nomenclature

α_{enc}	Encoding coefficient
α_{mod}	Modulation coefficient
Δa_{inj}	Semi-major axis injection error
Δi_{inj}	Inclination injection error
Δi_{sec}	Secular variation of the inclination of the orbit in 1 year
ΔV_{decay}	Semi-major axis correction cost
ΔV_{EOL}	End of life manoeuvres cost
ΔV_{inc}	Inclination correction cost
ΔV_{inj}	Injection correction cost
ΔV_{tot}	Total manoeuvres cost
$\dot{\theta}$	Slew angular rotation rate
ϵ_{BOL}	efficiency of BOL
$\frac{E_b}{N_0}$	Energy per bit over Noise density
$_{rx}$	Receiver gain
$_{tx}$	Transmitter gain
$Ł_{cable-rx}$	Receiver cables losses
$Ł_{cable-tx}$	Transmitter cables losses
λ_{tx}	Transmitter wavelength
μ_{amp}	Efficiency of the amplifier
μ	Packaging efficiency
ρ	Density
σ	Yield Strength
θ	Slew angular rotation
Θ_{rx}	Receiver bandwidth

A_{SA} Solar array surface

B_{mod} Modulation index

C_{fin} Effective battery capacitiy

C_{real} Actual battery system capacitiy

E_d Energy density

E_s Specific energy

f_{tx} Transmitter frequency

I_0 Sun irradiance

I_d Inherent degradation

I_{sp} Special Impulse

k Boltzmann constant

L_{atm} Atmospheric losses

L_{life} Lifetime degradation

L_{mod} Modulation losses

L_{point} Pointing losses

L_{space} Free space losses

m Mass

m_{batt} Batteries mass

$m_{prop-safe}$ Propellant mass needed in safe mode

m_{SA} Solar array mass

n_{orbits} Number of orbits elapsed between every desaturation

$N_{parallel}$ Number of paraller strings

P_{BOL} Specific power at BOL

P_{carr} Carrier power

P_{EOL} Specific power at EOL

P_{in} Power input for the antennas

P_{rx} Power received by the antennas

P_{SA} Power requested for solar arrays

$P_{science}$ Maximum internal power consumption

P_{sup} Supply Pressure

P_{tot} Total power at launch

P_{tx} Power transmitted by the antennas

R_{down-X} Datarate of download in the X-band

SNR_{carr} Signal to Noise Ratio carrier

SNR_{marg} Signal to Noise Ratio marginal

SNR_{min} Signal to Noise Ratio minimum

T Thrust

T_d Power request in daylight

T_d Spacecraft time in daylight

T_e Equivalent temperature

T_e Power request in eclipse

T_e Spacecraft time in eclipse

T_{life} Mission duration

th Thickness

V_{batt} batteries volume

V_{cell} Cell voltage

V_{tank} Volume in tank

X_d Line efficiency in daylight

X_e Line efficiency in eclipse

Δt_{des} Desaturation period

A-DCS3 Argos Advanced Data Collection System

A_{panel} Area of the solar panel

AKE Average Knowledge Error

AMSU-A Advanced Microwave Sounding Unit-A

AOCS Attitude and Orbit Control Subsystem

APE Average Performance Error

ASCAT Advanced SCATterometer

AVHRR/3 Advanced Very High Resolution Radiometer

B Blow-Down Ratio

BER Bit Error Rate

BOL Beginning of life

BSP Housekeeping and pyrotechincs unit

C Required capacity

CBS Standard Bus Couplers

CCSDS Consultative Committee for Space data systems

CCU Central Communication Unit

CDA Command Data Acquisition station

ConOps Conceptual operation

CPDU Command Pulse Direct Unit

DBU Digital Bus Units

DoD Depth of discharge

dpy degradation per year

DSP Digital signal processor

EAIM Associated monitoring and command unit

EDR Decoding and reconfiguration Unit

EIRP Effective Isotropic Radiated Power

EIU Electrical Interface unit

EOL End of life

EPS Electric power subsystem

FDF Flight Dynamics Facilities

FMU Formatting and multiplexing unit

GNSS Global Navigation Satellite System

GOME-2 Global Ozone Monitoring Experiment–2

GRAS GNSS Receiver for Atmospheric Sounding

GSN GRAS Support Network

h_{max} Max angular momentum

HIRS/4 High-resolution Infrared Radiation Sounder

HKTM spacecraft

I_{max} Max inertia moment

I_{min} Min inertia moment

IASI Infrared Atmoshperic Sounding Interferometer

ICU Instrument control unit

ICU Intelligent Control Units

LEO Low Earth orbit

LEOP Launch Early Operation Phase

LTAN Local Time of the Ascending Node

m Magnetic moment

MAC Magnetorquers

MetOp-A Meterological operational polar satellite

MHS Microwave Humidity Sounder

MLI Multi-Layer-Insulation

n Number of orbits elapsed between each semi-major axis correction manoeuvres

Ni-Cd Nichel-Cadmio

NIU NOAA Interface unit

NOAA National Oceanic and Atmospherical Administration

nom Nominal

NPU MHS protocol conversion unit

OBDH On-board Data Handling

PCM Payload module computer

PCU Power control unit

PLM Payload Module

PMC Payload Module Computer

prop Propellant

PSO On-orbit Position

RBI Standard Remote Bus Interface ASICs

RPE Relative Performance Error

RTU Remote Terminal Units

S/C Spacecraft

S/S Subsystem

s/s Subsystem

S&R Search and Rescue Processor and Repeater

SA Solar array

SAS Sun Acquisition Sensors

SEM Space Environmental Monitor

Si Silicon

SIOV Satellite In-Orbit Verificatio

SM Service Module

STD Digital Infra-Red Earth Sensor

SVM Service Module

T_d Drag torque

T_m Magnetic torque

t_m Duration in years of the nominal mission

t_{des} Time spent to desaturate the reaction wheels

T_{gg} Gravity gradient torque

T_{mag} Magnetorquers torque

T_{SRP} Solar Radiation Pressure torque

T_{tot} Total torque

TCH TeleChergement

TCS Thermal Control Subsystem

TM/TC Telemetry and Telecommand

tot Total

Contents

List of Figures

List of Tables

Chapter 1

ChangeLog

ChangeLog	
§ 2.6.1	pp. 6 : extended examination of the correlation of p\l to the ConOps\phases
§ 2.8	pp. 8 : better analysis of ΔV request during the Routine operation
§ 3.1	pp. 10: Ulterior analysis of the PS configuration pp. 11: Tank placement justification and ADCS comments removal
§ 3.2.1	pp. 13: Added justification for the value used of I_s
§ 3.3	pp. 13-14:Added justification for the value used of B_{nom} and correction of the mass of the Titanium tanks
§ 4.2.1	pp. 18-19 : gain, the value of total power for the subsystem, other correlated values corrections and revaluation of bandwidth and *SNR*
§ 4.2.2	pp. 19-20 : gain, the value of total power for the subsystem, other correlated values corrections and revaluation of bandwidth and *SNR*
§ 4.2.3	pp. 21 : typing error on the type of gain and revaluation of bandwidth and *SNR*
§ 6	pp.29 : explanation of sizing margin
§ 6.2	pp.30-31 : correction of Q_{IR} and rational of final result
§ 8.2.2	pp. 44 : better comparison with real mounted microprocessor

Table 1.1: ChangeLog

Chapter 2

Preliminary Analysis

2.1 Understand the mission high level goals[1]

Met-Op A is the first of a series of 3 satellites built for a program in collaboration between ESA and EUMSAT. The high-level goals of MetOp-A are:

1. **Improved Weather Forecasting**: one of the main purposes of this satellite is climate analysis aimed at providing information on the weather as accurate as possible. The satellite carries a suite of instruments that measure various atmospheric parameters such as temperature, humidity, and wind speed. Data collected from these instruments are used to improve the accuracy of weather forecasting models and to give more accurate weather warnings.

2. **Climate and Environmental Monitoring**: another purpose of MetOp-A is to collect information on the climate, atmosphere and environmental conditions of the Earth in order to formulate models that predict future climate advancement and understand changes in the environment of the planet and to help manage natural resources.

3. **Disaster Response**: MetOp-A plays a critical role in disaster response efforts. The program provides data on weather patterns and environmental conditions, which can be used to predict and respond to natural disasters such as hurricanes, floods, and wildfires. In addition to this function the satellite also allows to transmit distress signals from users in difficulty to search and rescue centres, and locate the source.

4. **Operational Support**: thanks to its instrumentation MetOp-A also provides support to naval units and aircraft providing real-time weather information.

Summarizing, the main goal of MetOp-A is to provide accurate, reliable, and timely data on weather patterns, environmental conditions, and climate change to help improve the understanding of the atmosphere of the Earth and to support decision-making related to natural resources management, disaster response, and other important issues.

2.2 Identify mission drivers, if any

- The S/C shall orbit in a *Sun-Synchronous Orbit*[4]:
  this kind of orbit is the perfect choice for a weather satellite because the illuminated surface every revolution is almost the same, helping with the observation.

- The S/C shall work for at least the first 5 years of its life:
  the lifetime of the satellite could be considered as a driver, since it was intended initially to launch the MetOp-A and shut it down after 5 years to launch MetOp-B[2].
- The launch date shall be such that the mission could respect all the deadlines:
  it has been considered this as a driver for 2 particularly reasons
  1. A delay in the launch involves an increase of the costs of the mission.
  2. One of the MetOp-A purposes was to support and then substitute the older NOAA-18[3], whose operational life should have ended in 2007.

2.3 Perform the mission functional analysis[4]

1. **Escape thrust from the orbit of the Earth.** Provide the necessary thrust to escape from the Earth and reach the prescribed orbit.
2. **Orbit injection manoeuvres.** Once reached the prescribed altitude, the satellite needs a delta-v for the injection in the final polar orbit.
3. **Orbit maintenance and navigation system.** Since it works in LEO orbit the effects due to the terrestrial magnetic field and Earth oblateness are significant, the satellite needs constantly a monitoring of its position and a control torque to keep it aligned with the desired configuration.
4. **Acquisition on atmospheric properties.** Measurements at various altitudes of atmospheric humidity, rain, snow, hail, sleet, chemistry, radiation, energy balance and temperature with a continuous scanning. Detailed 3D picture of the atmospheric content and profile of certain atmospheric components.
5. **Ocean data acquisition.** General ocean circulation and fluxes of heat, momentum and gases, wind speed and direction.
6. **Gravity and magnetic field data acquisition.**
7. **Hydrology and cryosphere data acquisition.** Day and night imaging of land, measurements of sea surface temperature, water cycle, continental snow and mountain glaciers, land cover, soil moisture, vegetation.
8. **Broadcast service provision.** Provides a continuous broadcast of its meteorological data to the worldwide user community, so that any ground station in any part of the world can receive local data when the satellite passes over that receiving station.
9. **Search and rescue tracking.** Availability to receive an emergency message from the Earth and transmit it to the local user terminal. Global coverage, twice daily.
10. **Communication with ground station.** During the available time window of telecom coverage, the satellite can send the scientific data to the ground station.
11. **Space environment tracking.** Provides information on solar activity and space weather which may affect the satellites and instruments.
12. **Data Collection.** Data storage inside an onboard memory.
13. **End-of-life operation.**

2.4 Identify its main phases

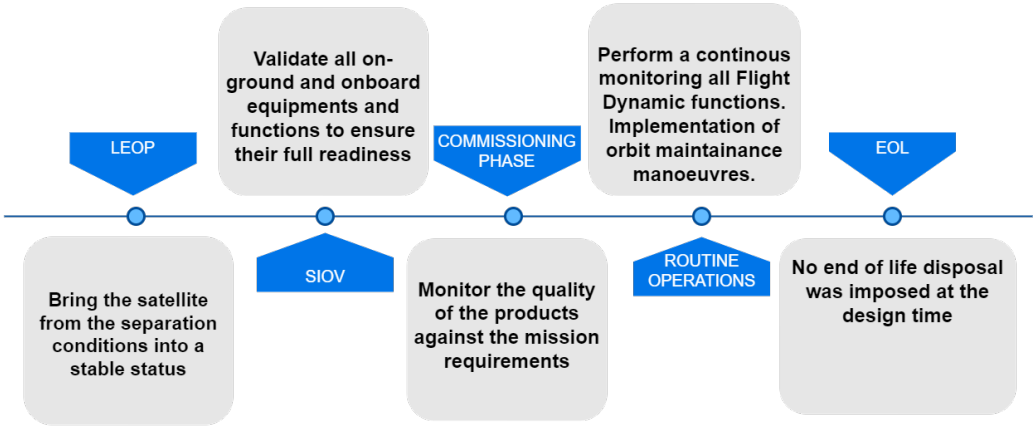

Figure 2.1: Main phases

2.5 Link phases to ConOps and functionalities[22]

1. **Launch & Early Operation Phase.**
   - Nominal pointing is acquired.
   - Solar panel and all antennas are deployed.
   - No major anomaly on-board is present.
   - Satellite is on an orbit drifting smoothly toward the operational one (target time 14 days).
   - Routine TCH (TeleCHargement, Telecommand) are on-board.
2. **SIOV (Satellite In-Orbit Verification)**
   - Quality of radiometric data from CDA (Control and Data Acquisition) and accuracy of orbit determination.
   - Behaviour of the on-board clock and accuracy of OBTUTC (On Board Time and Coordinated Universal Time) correlation.
   - Behaviour of the sensors and pointing stability of the satellite. Moreover, a drift stop manoeuvre was executed within the second week of SIOV to acquire the reference ground-track for commissioning. That permitted to fully validate the manoeuvring capabilities in FDF of all the backup units was validated.
3. **Commissioning phase.**
   - Orbit determination and propagation.
   - OBTUTC correlation.
   - Satellite pointing.
   - AOCS (Attitude and Orbit Control Satellite) TCH.
   - Geometric and vector products operations needed to continuously perform these monitoring activities during routine were moreover developed.

4. **Routine Operations.**

   - 3 operational sequences are executed daily to fulfil with the need of updating the SVM (SerVice Module) TCH twice a day and to update the mission planning and GRAS (GNSS Receiver for Atmospheric Sounding) support network (GSN) products once a day.
   - Events for mission planning are generated weekly and re-synchronised daily to the latest values of the ascending node crossing time.
   - SVM TCH must be generated considering geocentric pointing and not considering any manoeuvre in the future up to the day of the manoeuvre itself.
   - Mission planning and GSN products are generated considering estimated attitude (nominally Yaw Steering Mode - YSM) and manoeuvre prediction 3 days in the future.

5. **De-orbiting phase and EOL (End Of Life)** No End-of-life disposal was imposed at design time (late 90's), however, the following phases have been implemented:

   (a) Preparation of the ground segment for the de-orbiting operations, and reconfiguration of the spacecraft for the environment conditions it will have to face during the de-orbiting.

   (b) De-orbiting of the satellite performing negative in-plane maneuvers.

   (c) Passivation of the propulsion subsystem.

   (d) Complete passivation and switch-off of the satellite.

2.6 Understand the on board scientific instruments primary utilisation[5]

MHS[6]: is a self-calibrating, cross-track scanning, five-channel microwave, full-power radiometer designed to collect information on various aspects of the atmosphere and surface of the Earth, especially for measure the specific humidity.

AVHRR/3[7]: is an across track scanner that senses the outgoing radiation of the Earth, from horizon to horizon in six channels, principally for monitoring of cloud cover, sea surface temperature, ice, snow and vegetation cover characteristics, but also for natural disaster monitoring.

A-DCS3[8]: made for the collection and dissemination of ocean data, in fact it consists of two units, RPU (Receiver Processing Unit) and TXU (Transmit unit).

S&R[9]: is an help to search and rescue authorities relaying distress signals from users in difficulty to search and rescue centers and locate the source.

SEM[10]: provides information on solar activity and space weather which may affect the satellites and instruments, collect data for the determination of auroral activity measuring the electron and proton integral directional flux.

AMSU-A[11]: is a multi-channel microwave radiometer, designed to obtain temperature profiles in the upper atmosphere (especially the stratosphere), providing information on atmospheric water in all of its forms, using oxygen absorption bands/lines for atmospheric temperature sounding.

GOME-2[12]: is an optical spectrometer, used to get a detailed picture of the total atmospheric content of ozone and its vertical profile in the atmosphere. That spectrometer provide also the total amount of gasses (nitrogen dioxide, sulphur dioxide, water vapour, oxygen, etc) in atmosphere.

GRAS:[13] is an instrument that uses the high quality radio signals from GPS navigation satellites, occulting the Earth atmospheric limb, through a tangential path through the atmosphere of the Earth, to provide stratospheric and tropospheric temperature and humidity using the NWP (Numerical Weather Prediction) models.

ASCAT[14]: is a Scatterometer that measures wind speed and direction over the oceans, made by a real aperture radar and using vertically polarised antennas.

HIRS/4[15]: is a 20-channel infrared scanning radiometer that uses CO_2 absorption bands for temperature sounding, providing calibrated vertical profiles of temperature and humidity.

IASI:[16] is the main payload instrument, whose purpose is supporting numerical weather prediction (NWP), providing information on the vertical structure of the atmospheric temperature and humidity in an unprecedented accuracy of 1K and a vertical resolution of 1km, measuring in the infrared part of the electromagnetic spectrum at a horizontal resolution of 12km over a swath width of about 2,200km.

2.6.1 Correlate p\l to ConOps\phases

The connection between the phases and the payload functions is reported in the following list:

- Launch & Early Operation Phase (LEOP), the payload instruments are kept off to save battery energy;
- Satellite In-Orbit Verification (SIOV) phase, the Payload Module is switched in its operational mode and all the instruments are tested, allowing the science data continuity, format and validity, using the SIOV ground tools;
- Commissioning phase, all the instruments remain switched-on collecting the first data. During this phase, using the data collected, a specific strategy for IASI has been defined to improve the stability and the performance, ;
- Routine Operations phase, all the instruments have their nominal functioning and perform the operations for which they were designed;
- De-Orbiting and End of Life phase, all the instruments have completed their operations and are switched-off in order to complete the passivation of the satellite.

In order to sum up these correlations, a condensed table has been presented here 2.1:

PHASES	INSTRUMENT
Launch & Early Operation Phase	[-]
SIOV (Satellite In-Orbit Verification)	Testing all the $p\backslash l$ instruments
Commissioning phase	First data collect and IASI strategy definition
Routine Operations	Normal operation time for $p\backslash l$
De-orbiting phase and EOL (End Of Life)	Switch-off of $p\backslash l$ instruments

Table 2.1: Phases to instruments relations

2.6.2 Correlate goal-to payloads functions

In order to correlate goal-to payloads functions, the following table has been presented 2.2 :

GOAL	INSTRUMENT
Improved Weather Forecasting	MHS: Specific Humidity measurement AVHRR/3: Cloud Information AMSU-A: Temperature profile and humidity measurement GRAS: Temperature and humidity profiles ASCAT: Wind information HIRS/4: Temperature and Humidity measurement IASI: Vertical temperature and humidity profile
Climate and Environmental Monitoring	MHS: Specific Humidity measurement AVHRR/3: Cloud Information A-DCS3: Wildlife, Ocean, Atmospheric Monitoring SEM: Solar activity and Space weather information (for Aurora determination) AMSU-A: Temperature profile and humidity measurement GOME-2: Vertical ozone profile and Ozone content GRAS: Temperature and humidity profiles ASCAT: Wind information HIRS/4: Temperature and Humidity measurement IASI: Vertical temperature and humidity profile
Disaster Response	MHS: Specific Humidity measurement AVHRR/3: Cloud Information A-DCS3: Wildlife, Ocean, Atmospheric Monitoring S&R: Relay distress signals receiving AMSU-A: Temperature profile and humidity measurement GRAS: Temperature and humidity profiles ASCAT: Wind information HIRS/4: Temperature and Humidity measurement IASI: Vertical temperature and humidity profile
Operational Support	AVHRR/3: Cloud Information ASCAT: Wind information

Table 2.2: Goal to payloads relations

2.7 Start correlating functionalities-phases trajectory design (MA understanding)

1. **Launch and early operation phase**
   The MetOp-A was launched from the Baikonur Cosmodrome [17] which is located at 45.6°N latitude and 63.4°E longitude in the flat grasslands of Central Asia in the former Soviet Republic of Kazakhstan. It has been chosen because it has a continental climate, with long, cold winters and hot, dry summers and because of its hytorical importance, in fact many Russian manned missions have lifted off from there, as well as geostationary, lunar, planetary, and many ocean surveillance missions. The spacecraft was delivered to the cosmodrome by air and integrated with the *Fregat* stage inside a modern payload processing facility.

2. **Routine operation**
   It has been chosen a *Sun Synchronus* polar orbit (*Local Time of the Ascending Node (LTAN)* at 21:30 hours), *mean altitude = 817 km*, *inclination = 98.704o*, *repeat cycle = 29 days (412 orbits)*. The polarity of the orbit reduces the distortion caused by the rotation of the planet while the altitude of the orbit guarantees an optimal observation of the planet and gives an orbital period of 101.4 min that allows more observation in a day. The LTAN of 21h 30min is imposed for the correct functioning of the Global Ozone Monitoring Experiment (GOME) instrument

3. **De-orbiting phase**
   No De-orbiting trajectory design has been considered since initially the satellite should have been switched off.

2.8 Start reverse the trajectory design per phase towards the Dv budget justification and retrieval

1. **Launch and early operation phase** :
   After the launch the upper stage of the launcher separates and subsequently generates a first burn of 1209.35m/s which transfer the upper stage and the satellite to the final separation orbit. With a second burn of 182.1m/s the upper stage enters the final orbit and then the separation occurs, leaving the MetOp-A on its orbit after 68min 59sec from lift-off.[18]

   After separation from the launcher *Fregat* upper stage, the satellite entered an automated sequence which allowed to initialize its in-orbit operations. At the injection, a Delta-V of 32.3m/s has been considered to compensate for injection errors.This value has been computed assuming that the maximum errors in the orbital parameters are: 35km as maximum variation between the nominal semi major axis and the one obtained after the injection; 0.02deg as inclination change after the injection. The value computed results much larger than the actual Delta-V used for injection (approximately 2m/s [22]) thanks to a very accurate operational orbit injection.

2. **SIOV** : To optimize the maneuver strategy EUMETSAT-CC allowed to freeze the eccentricity when performing an IP drift stop manoeuvre with a Delta-V below 20 cm/s.[22]

3. **Routine operation** :
   The long-term inclination control strategy to nullify the effect of the Sun gravity field foresees the execution of one out-of-plane manoeuvre campaign (each consisting of one or two burns) every year, preferably around the autumn longer-eclipse season. To compute the total ΔV used for the Routine Operation phase, the contribution of the thrusters for compensating two different phenomena it has been considered:

   - The ΔV_{decay}, related to the semi-major axis correction and caused by the drag encountered by the satellite during its orbital period. A certain deviation of the semi-major axis of the orbit will be generated. This cost is computed as the ΔV of an Hohmann tranfer between two circular orbits (the nominal one and the decayed one) [25];
   - The ΔV_{inc}, associated to the inclination correction manoeuvre and computed as the sinusoidal function of the secular variation of inclination = 0.05° [25];

Considering the computation of the ΔV used for the correction of the trajectory, the value of $6.9 m/s$ can be used as approximation.

In April 2008 [20] the first inclination correction of around $70 mdeg$, corresponding with a ΔV of the order of 10m/s, was required. Considering the quite large mass of the satellite (more than 4 tons) and the very limited thrust available (around 36 Newton) around 18 minutes of continuous propulsion would have been needed. Due to instrument illumination constraints the entire manoeuvre phase must be carried out within eclipse. Subtracting from the eclipse time (around 30 minutes) the time needed for slew and anti- slew (each of them of the order of 11 minutes), it became evident that the required inclination correction could not have been provided by a single burn. Execution of two burns was then selected. In order to maximise the manoeuvre efficiency, the anti-velocity plate was selected: its pitch control thrusters being fully aligned with the anti- velocity direction, this plate provides better performances. A negative rotation around the satellite's Z axis is therefore applied before the manoeuvre. The rotation of the platform to the desired attitude for the manoeuvre and the return to geocentric attitude mode, is performed by the platform in the so-called Orbit Control Mode (OCM). During this mode, the attitude control of the spacecraft is performed with thrusters. The results for the thrusters used in this case include a modification which added new parameters to them: the net along-track(DeltaV $= -0.099$) and cross-track(DeltaV $= -0.070$)[20]. The generation of the manoeuvre telecommand (TCH) then takes these values into account to subtract them from the commanded manoeuvre: the cross-track component is adjusted with the commanded number of pulses, and the along-track one with the commanded slew rotation. The spacecraft also uses fuel to keep the LTAN in a 2 minutes boundary to keep sun-calibration geometry for the Global Ozone Monitoring Experiment (GOME) instrument.

4. **De-orbiting phase** : The de-orbiting phase begins with the lowering of the satellite from a mean altitude of $817 km$ to $580 km$ and uses 15 maneuvers conducted over 10 days. When it reaches the South pole the spacecraft performs an upside down maneuver that enable EUMETSAT teams to improve the accuracy of weather and climate data. After this the MetOp-A is dragged by the atmosphere and looped down by the Earth gravity until it finally disintegrates.[21]

Chapter 3

Propulsion subsystem

3.1 Propulsion subsystem architecture

The MetOp-A is a three-axis stabilized satellite. For the primary propulsion two branches of eight 23.5 N thrusters are used. The pointing knowledge is: 0.07 (x-axis), 0.10 (y-axis), 0.17 (z-axis). [27]

Prime	Redundant	Torque	Thrust
1	2	+Y	
3	4	-Y	
5	6	-X	
7	8	-Z	-Y
9	10	+Z	-Y
11	12	+X	
13	14	+Z	+Y
15	16	-Z	+Y

Table 3.1: Thruster [27]

The eight thrusters allow the generation of torque in all three axis and of propulsion in the ±Y axis and each one is designed to deliver a nominal thrust of 22.7 N at the beginning of life. (Figure 3.1). This configuration has been chosen to allow a good pointing accuracy (in combination with the secondary attitude and control s/s) and the station keeping, that is composed by the satellite positioning with a rotation around its yaw axis (slew) and an out-of-plane manoeuvre. Besides, instrument illumination conditions impose that the satellite can only be slewed within eclipse conditions. In a first manoeuvre campaign, the slew was designed as two burns with a very small separations of 15 hours; however, in a a secondary analysis, the slew has been designed as a single manoeuvre composed of five segments: slew start and stop, main propulsion and anti-slew start and stop; that has shown much better performances, permitting to obtain more reliable calibration factors.

The Cartesian reference frame indicated in the figure depicts the MetOp satellite body frame of reference in which –Z points toward the Earth center. The rectangular box on the left in Figure 3.1 is a rough representation of the MetOp spacecraft that complements the thruster configuration schematics on its right. The green patches signify the location of the thruster pairs grouping on the spacecraft. The thrusters are aligned to minimize potential contamination of the spacecraft payload by the exhaust plume and not only for the needs of orbit control[30]. The thrust provided is in the form of pulses designed to operate at 8 Hz. Throughout the maneuver phase, the attitude control thrusters are actively controlled by the AOCS to correct

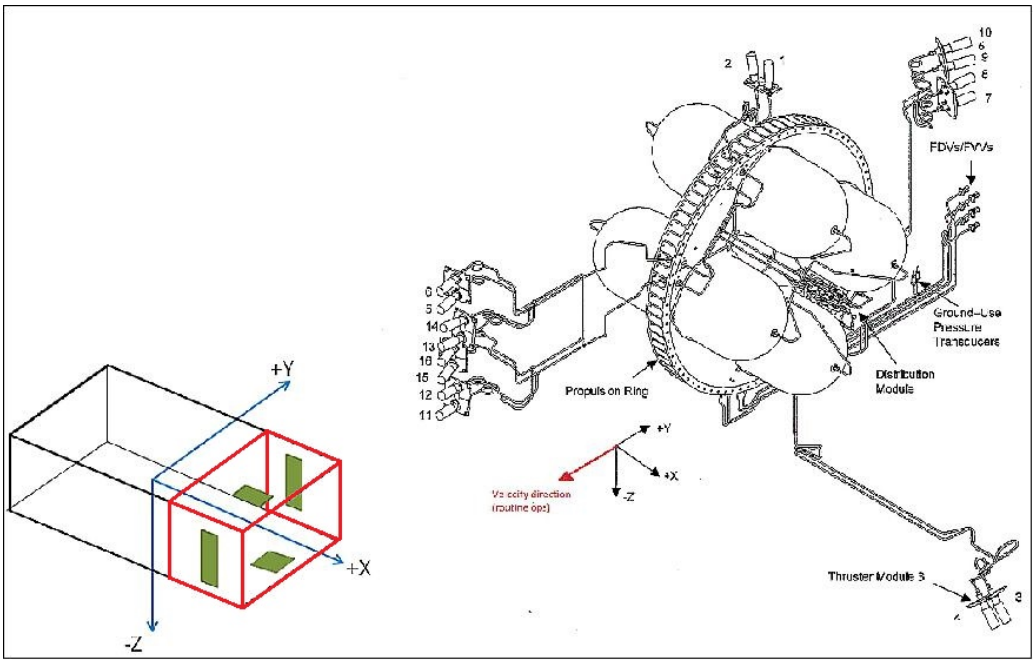

Figure 3.1: Thrusters [27]

the attitude pointing due to torque imbalance created by the propulsion and coupled thrusters. Due to the requirement of the mission the propulsion system must be restartable, therefore the solid propulsion has been excluded. Bi-propellant system and Dual mode system have not been considered in the design since the magnitude of the thrust produced is much higher than the one needed; while Arcjet and Resistojet have not been taken into account because they produce a lower thrust than the one needed. For these reasons, a monopropellant propulsion system has been selected and implemented. The tanks have been positioned in the centre of the Service Module (indicated with the red path in Figure: 3.1) in order to keep the centre of mass close with the geometrical one.

Secondary attitude control dynamics is provided by three 40 Nms reaction wheels, by two magnetotorquers which are able to generate a 315 $[Am^2]$ magnetic moment, and by the associated monitoring and command unit.

The orbit control is achieved by the execution of two types of manoeuvres in order to keep the distance to the ground-track and the LTAN within a predefined dead-band. In-plane manoeuvres have been implemented to change the semi-major axis (and eccentricity) which allow to control the ground track deviation from the reference orbit at the Earth Equator. Out-of-plane manoeuvres have been used to correct the inclination, allowing to control the deviation from the reference ground-track at high latitudes as well as the drift of the ascending node and its local time. No fuel was initially allocated to de-orbiting, since no End-of-life (EOL) disposal was imposed at design time but, thanks to a very accurate injection into the operational orbit and to a close to optimal orbit maintenance, together with the fact that no major anomaly at platform level has occurred, a large amount of fuel has been saved in comparison with the design case during the first seven years of operations. This fuel has been allocated to extend the satellite lifetime and to put the satellite in a faster-decaying orbit which will result in an earlier atmospheric re-entry of around 25 years.

The total ΔV_{tot} budget has been assessed breaking it down into different components [25]:

$$\Delta V_{tot} = \Delta V_{decay} + \Delta V_{inj} + \Delta V_{inc} \tag{3.1}$$

ΔV_{decay} is related to the semi-major axis correction; a certain drag model has been used for satellites in LEO orbit, through which the deviation of the semi-major axis and of the

orbital period for one single orbit have been calculated. Using an imposed tolerance on the displacement from the nominal orbit ground track at the equator, the number of orbits n which have to elapse between the manoeuvres has been recovered. The total variations of the semi-major axis and of the orbital period after the number of orbit n have been exploited in order to evaluate the ΔV_{decay}, found as the ΔV of an Hohmann tranfer between two circular orbits (the nominal one and the decayed one). This cost is about one manoeuvre; thanks to the n value, we can compute how many manoeuvres have to be provided for the entire time of the mission.

ΔV_{inc}, cost associated to the inclination correction manoeuvres, has been estimated using the following formula:

$$\Delta V_{inc} = 2sin(\frac{\Delta i_{sec}}{2}) \cdot t_m \tag{3.2}$$

In which Δi_{sec} corresponds to the secular variation of the inclination in one year (0.05° [24]), and t_m is the number of years of the whole mission (5 years). ΔV_{inj} has been computed using an Hohmann transfer with plane change, between the nominal orbit and a modified orbit considered a certain injection error ($\Delta a_{inj} = 35km$, $\Delta i_{inj} = 0.02°$[25]). The overall ΔV_{tot} and its breakdown are reported in the following table 3.2:

$\Delta V_{decay}[\frac{m}{s}]$	$\Delta V_{inc}[\frac{m}{s}]$	$\Delta V_{inj}[\frac{m}{s}]$	$\Delta V_{tot}[\frac{m}{s}]$
2.5	4.4	32.3	39.1

Table 3.2: Mission's velocity budgets.

The value of the ΔV_{tot} found corresponds to an amount of propellant mass equal to 150 *kg*, which is more or less half of the amount of propellant used in the real mission, equal to 316 *kg*, as it can be seen from [28]. 150 *kg* of the total 316 *kg* of propellant have been saved for contingency in the real mission, in which, at the beginning of 2014, 198 *kg* were still usable. This amount of propellant was exploited for the End-of-Life manoeuvres. Considering the End-of-Life manoeuvres in the computation of the ΔV_{tot} budget, and comparing the new amount of propellant that this new ΔV_{tot} leads, a consistent result has been found. The ΔV_{EOL} has been evaluated assuming an Hohmann transfer between the nominal orbit and a 600 *km* of altitude orbit, and it corresponds to 40.9 *m/s*. The new value of the ΔV_{tot} results as 80 *m/s*, which led to 301.9 *kg*. This is the evidence that the amount of propellant saved for contingency has been used for the End-of-Life manoeuvres; the result, obtained embedding these manoeuvres in the evaluation of ΔV_{tot}, are compliant with the actual onboard amount of propellant.

3.2 Propulsion subsystem reverse sizing

3.2.1 Propellant selection and masses

The propellant selected for the MetOp-A mission is the Hydrazine (N_2H_4), an hypergolic and remarkably toxic propellant highly used in low-thrust and high precision engines for the positioning on orbit of satellites and space probes. The Hydrazine was selected because to:

- **Simplicity** : it is a monopropellant, so it's necessary only it to generate thrust.
- **In-depth Knowledge** : the properties of hydrazine are well-known due to its extensive use in spaceflight applications.
- **Components** : the extensive usage of hydrazine systems has led to the development of a strong ecosystem of components and expertise. Hydrazine propulsion systems are regularly modified utilizing the parts that are readily available for particular uses.

- **Cold Restarts** : these systems have the benefit of frequently being capable of several cold starts.
- **High Specific Impulse** : in comparison with the dimension of the propellant system.

Starting from the data collected, the evaluation of the choice on propulsion S/S has been done, with the purpose to analyse the propellant, engine and pressurizer implemented in the real mission[6] [7].

T Range $[N]$	*Nominal* I_{sp} *Range* $[s]$	*Supply* P_{sup} *Range* $[bar]$	*Propellant* $[-]$	*Total Impulse* $[Ns]$
$7.9 \div 24.6$	$222 \div 230$	$5.5 \div 24$	N_2H_4	$> 517,000$

Table 3.3: Performance of Ariane 20 N thruster

Using the nominal values reported in the table 3.4, the *Tsiolkovsky Equation* has been used to recover the mass of propellant, which has been computed considering a total manoeuvre cost with a 100% margin, using a conservative approach. From this evaluation the m_{prop} results as 289.16 kg. Considering the increment of m_{prop}, due the addition of margins (3% to take into account ullage, 2% for residuals and 0.5% for the loading uncertainty), the total value of mass is 301.9 kg, which is a consistent value with the actual propellant mass on-board of 315 kg, if decreased of the margin of residual propellant (+2%)[8].

m_{launch} $[kg]$	I_{sp} *nominal* $[s]$	$\rho_{N_2H_4}$ $[\frac{kg}{m^3}]$	ΔV_{tot} *real* $[\frac{m}{s}]$	ΔV_{tot} *margined* $[\frac{m}{s}]$	m_{prop} $[kg]$
4093	225	1032	79.99	159.98	301.9

Table 3.4: Nominal Values for mass sizing

For the nominal specific impulse ($I_{sp}nominal$), a mid-value has been taken to be representative of the real situation and avoid edge cases due to the minimum and maximum possible impulse provided by the engine.

3.3 Tanks and feeding strategy

The choice of using a *Blow-Down* feeding strategy instead of a *Regulated* one is justified by the propellant selected for the mission and for simplicity reasons. Since the propulsion system is a monopropellant, a *Regulated* system has been rejected due to its complexity and because it is typically suitable for a bipropellant propulsion system. The drawback of using a *Blow-Down* system is that the pressure of the pressurant reduces with time as well as the capability to keep the feeding pressure for the propellant constant. However, this effect is restricted by the use of multiple tanks. The *Blowdown ratio* has been chosen as 4.5 after comparing the typical values used in the literature[83] with the values actually used in reality.[13]

Concerning the tank sizing, the *Helium* [10] has been considered as pressurizer. A number of tanks equal to four have been used in the computation. This brought to the volume of the tanks for both propellant and pressurizer. In the table 3.5 are reported the main variables used in the evaluation.

m_{prop} $[kg]$	B *range* $[-]$	B_{nom} $[-]$	$\rho_{N_2H_4}$ $[\frac{kg}{m^3}]$	R_{He} $[\frac{J}{kg*K}]$	γ_{He} $[-]$	P_{tank}*range* $[bar]$
301.9	4 ÷ 6	4.5	1032	2077.3	1.67	7÷31.5

Table 3.5: Nominal Values for tanks

Instead of one or two bigger tanks, four tanks have been chosen for space and disposition reasons. The choice of four relatively smaller tanks, at first sight, permits an easily location, and, if a smaller number of tanks was considered, a leakage issue would have been significant. Furthermore, implementing four tanks allows to have a better distribution of mass. Taking into consideration the material analysis for the tanks, two different metal alloys have been compared, a Titan-based (*Ti-6Al-4V*) and an Aluminium-based (*Al7075*). The thickness and masses of an hypothetical configuration of 4 spherical tanks made of the already mentioned alloys has been used in the comparison. The table 3.6 shows the results.

Materials	ρ $[\frac{kg}{m^3}]$	σ^Y $[MPa]$	th $[mm]$	m_{tot} $[kg]$
Al7075	2810	503	0.915	11.065
Ti-6Al-4V	4430	9500	0.484	9.209

Table 3.6: Comparison between materials

Since the purpose is to save mass, the Titan-based alloy has been selected as tank material, because of the reduced thickness of the tanks, thanks to the higher *Yield Strength*. The results are coherent also looking at the common use of titanium in small tank for satellites. [14] Without a reference on the actual tanks and on the pressurization system implemented in the real mission, the theoretical properties of the selected tanks have been compared with the one related to a specific *hydralazine* diaphragm tank (PTD-96) [13], used in similar missions, in order to ensure an objective comparison, as it can be appreciated from the table 3.7. The conducted analysis reveals that the values obtained remain consistent with similar tanks, suggesting that these results are also coherent with the possible decisions taken by the *Metop-A* design team.

Tank	B_{nom} $[-]$	V_{tot} $[m^3]$	V_{tank} $[[m^3]$	P_{tank} $[bar]$	*Material* $[-]$
PTD-96	4.5	0,384	0.096	5.33÷24	Ti-6Al-4V
Tank Evaluation	4.5	0.418	0.1045	7 ÷ 31.5	Ti-6Al-4V

Table 3.7: Comparison between tanks

3.3.1 Pressurant selection and masses

The most used pressurizers in *Blow-Down* systems are *He* and N_2. A comparison between these two pressurizers has been done in order to justify the choice of *He* as pressurizer. The *Blow-Down* ratio, which fluctuates typically between 4 and 6, has been assumed as 4.5 from literature [15]. From this ratio, the initial and final volume of the pressurizer have been found. The pressure in the combustion chamber has been selected as 5 *bar*[6]. Considering the pressure losses related to the injection and feeding, the pressure that the pressurizer has to guarantee in the tanks at the end of the mission has been found. Summing the volume of the pressurizer and the volume of the propellant, which has been evaluated using the density of the hydrazine

P_c [bar]	$P_{tank-final}$ [bar]	$P_{tank-initial}$ [bar]	V_{press} $[m^3]$	V_{prop} $[m^3]$	V_{tot} $[m^3]$
5	7	31.5	0.0919	0.3218	0.4179

Table 3.8: Tank Parameters

and adding a 10% margin, the total volume of the tanks has been obtained, with a 1% margin. The main variables are reported in the following table:

Since the initial volume occupied by the pressurizer and the initial pressure that the tank should guarantee have been computed, it has been possible to obtain the masses of the needed He or N_2, exploiting the *Perfect Gas* law, and to compare their masses. The *Helium* mass ($0.47kg$) resulted to be 1/6 smaller than the *Nitrogen* one (3.33 kg). This result justify the choice to adopt *Helium* as pressurizer in order to save mass.

Chapter 4

Telecommunication,Telemetry and Control subsystem

4.1 TTMTC architecture [34]

The telecommunication system of the MetOp-A must sasitisfy the connection *satellite2ground* for both scientific data and telemetry&control. For this reason, two omnidirectional S-band coverage provide TT&C support (uplink 2 kbit/s, downlink 4 kbit/s), while instrument data is downlinked in X-band at a rate of 70 Mbit/s. The scientific data communication requires an high frequency since the data volume is much higher, therefore has been chosen the X-band with a frequency of 7.800 GHz. MetOp-A has been designed, also, with an onboard storage memory; the *Solid-State Recorder* is based on the Cluster and Envisat design, and has a capacity of 24 GB at end-of-life. This is sufficient for slightly more than one full orbit of data. The X-band subsystem provides a direct 70 $Mbps$ transmission link to ground during visibility periods, dumping the data stored during the previous orbit to ground. In addition to onboard recording and X-band downlink capabilities, MetOp supports the real-time broadcast of instrument data to local authorized users by the following means:

- LRPT (Low-Rate Picture Transmission) links with 72 kbit/s in VHF-band for selected instrument data.
- AHRPT (Advanced High-Rate Picture Transmission) links with 3.5 Mbit/s in L-band. The new AHRPT service (a WMO standard) enables regional users to receive all data relevant to their area in real time. Users operating existing HRPT stations will have to modify their stations to receive the "Advanced" MetOp data.

The TTMTC architecture is the following:4.1

Data type	**Frequency domain**	**Modulation scheme**	**Data rate**
TT&C uplink	S-band, 2053.4 MHz	NRZ/PSK/PM	2 kbit/s
TT&C downlink	S-band, 2230 MHz	SP-L/PSK/PM	4 kbit/s
Global data dump	X-band, 7.750-7.900 GHz	QPSK	70 Mbit/s
LRPT downlink	VHF-band, 137.1 MHz	QPSK	72 kbit/s
AHRPT downlink	L-band, 1701.3 MHz	QPSK	3.5 Mbit/s

Table 4.1: MetOp communication link

For the ground support segment point of view, the EPS (*EUMETSAT* Polar System) Ground Segment has been selected, giving all the facilities required to support the orbiting

MetOp and collecting the information for both normal and degraded mission modes. Its objectives are:

- To ensure that the satellite performs their mission nominally;
- To perform the ground operations to fulfil the global mission, acquiring and processing the global data received from MetOp-A and disseminating the processed data to the Eumetsat member states and to support the local data-access mission (HRPT/LRPT);
- To support MetOp for global data acquisition and telemetry, tracking and control during blind orbits.

The EPS ground segment contains the Eumetsat multi-mission dissemination system (EUMETCast) for near-realtime delivery to users of the global data and products derived from the MetOp data for the morning orbit. The core ground segment provides the following functions at the different sites:

- **Central Site**, includes all the functions for monitoring and controlling the satellite and the ground segment and located at Eumetsat headquarters in Darmstadt, Germany.
- **The Polar Site**, at Svalbard (NO, latitude 78^{o}N), hosts the CDA (Control & Data Acquisition) station that receives the MetOp recorder dump every orbit and command the satellite.
- **The BUCC (Back-Up Control Center) site**, close to Madrid, Spain, was created in case of major problems with the central site.

Visibility profiles allow contact periods varying between 4 and 12 minutes with a typical period of better than 10 minutes. Commands can be directly up-linked and executed during visibility periods or up-linked and stored on board for execution later.

Science data transmission to ground is ensured by three links:

- an X-band link to the CDA station at Svalbard to dump the SSR global data and for further forwarding via terrestrial transmission links to the EPS Central Site in Darmstadt.
- the HRPT and LRPT providing continuous data transmission to ground in VHF and L-bands for local users. On-board encryption of the LRPT and HRPT data prevents access by un-authorised users. The EPS Key Management Centre generates the encryption keys and distributes them via secure terrestrial links to registered local mission users.The HRPT service operates with a microwave link at L-band and broadcasts the full data content as recorded on board MetOp at 3.5 Mbps.

In the first part of the mission, when the payload is not already operative, the communication *ground2satellite* in S-band is firstly established. Once the satellite reaches the desired configuration, and instruments are switched on, it is possible to set the communication in X-band. Both communication lines will be active until the end-of-life of the satellite, when the payload will be switched off as well as the X-band connection, while The S-band one is still useful to control the TT&C of the satellite for the last manoeuvres.

Regarding the data volume, during the mean time window for the X-band, we can send maximum $42GB$, which is more than the maximum storage capability of the satellite. This allows to send properly all the scientific measurements and in addiction there is a temporal margin to establish a safe connection with the GS. While for the S-band the total data volume is $3.66MB$.

4.2 TTMTC reverse sizing

4.2.1 X-Band downlink

Due to the high number of instruments on-board, the amount of data needed to be transferred is significant (70 *Mbps*). To send this amount of data to ground, the X-Band has been chosen as frequency in the band of $7.750 - 7.900$ *GHz* to respect the Radio Frequency Regulation of the European Commission [39]. The Encoding method which has been adopted is the Reed Solomon Encoding, suitable for the high amount of Data that the satellite has to transfer [38]. The X-Band antenna has an horn structure [34]; a conservative approach has been adopted in order to recover the gain, therefore the lowest possible gain for this type of antenna has been selected, which corresponds to 5 *dB*. Horn antennas are very preferable in these applications since they can be built easily and provide low voltage standing wave ratios [40]. This horn antenna always points to the Earth to guarantee a proper communication.

Regarding the Ground Station selection, the Svalbard Polar Site has been chosen because its high northern latitude position benefits from the close proximity of orbit tracks at the poles and ensures visibility and commanding by the CDA for all MetOp daily orbits. The antennas of the Ground Station are capable to operate at the same frequency of the satellite X-Band antenna, and to handle the data rate received. Visibility profiles allow contact periods varying between 4 and 12 minutes with a typical period of 10 minutes. The amplification of the signal for the X-Band has been done using a Travelling Wave Tube Amplifier (TWTA), which has been implemented looking at the relatively higher efficiency with respect to other amplifiers, and at the high amount of data to transfer in such a small time window.

The system has been sized using the following variables 4.2:

P_{tot} $[W]$	P_{input} $[W]$	μ_{amp} [-]	BER_{TM} [-]	a_{enc} [-]	a_{mod} [-]
2175.6[34]	189.75	0.45[36]	1e-5[35]	1.14 [38]	2 [34]

Table 4.2: X-Band variables

The average power given by the solar panel on one orbit is 2175.6 *W*. This value has been reduced by the power consumed by the instrument (910.6 *W*), in order to obtain the amount of the average power given by the instrument (1265 *W*). The portion of the power assigned to the telecommunication *s/s* for meteorological satellite is selected as 189.75 *W*.. The efficiency of the amplifier has been selected from literature [35], and it gave a transmitted power of 85.39 *W*. The Minimum Energy per Bit to Noise Density $\frac{E_b}{N_0}$ has been estrapolated from the graph, using the BER as input and looking at the Reed Solomon Encoding curve [38], and it results as 5.5 *dB*. The sizing has been done using the dominant data rate for X-Band, which is 70 *Mbps*. The Real Data Rate has been obtained multiplying it times the ratio between the encoding coefficient α_{enc} and α_{mod}, and it results to 39.9 *Mbps*. The gain of the transmitting antenna has been selected as 5 *dBi* underestimating the value for a horn antenna and, instead, the gain of the receiving antenna has been found as 57.5 *dBi* from [41]. Concerning the evaluation of the Losses, the following values has been obtained 4.3:

$L_{cable-rx}$ [dB]	$L_{cable-tx}$ [dB]	L_{space} [dB]	L_{point} [dB]	L_{atm} [dB]
-2[35]	-2[35]	-192.9233	-0.0227	-0.05 [35]

Table 4.3: X-Band Losses evaluation

An average value has been selected for the cable losses for both receiver and transmitter. The losses associated to the distance have been evaluated assuming the maximum distance

between the satellite and the Ground Station. The losses linked to the pointing of the antenna have been computed using the typical pointing error of 0.01° and a beamwidth of 0.23°. The atmospheric losses have been assessed looking at the tables from literature[35]. From the losses and the Gain of the transmitting antenna, the EIRP has been computed and, consequently, the receiver power $P_{rx} = -113.68\ dB$. The system noise density, calculated using a sensor temperature of 150 K [41], the Energy per Bit to Noise Density and its margin have been computed and they are reported in the following table 4.4:

N_0 [dB]	$\frac{E_b}{N_0}$ [dB]	$(\frac{E_b}{N_0})_{min}$ [dB]	$Margin$ [dB]
-206.84	17.15	5.5	11.65

Table 4.4: System noise

Assuming the typical value of 78° for the Modulation Index, the Carrier Modulation Index Reduction is $-13.64\ dB$, so, the Carrier Power is $-127.32\ dB$. In order to have a SNR_{margin} higher than 3dB, a receiver bandwidth of 0.447 MHz has been computed. The following value of Signal To Noise Ratio have been obtained 4.5:

SNR_{car} [dB]	SNR_{min} [dB]	SNR_{margin} [dB]
23.02	20.00[42]	3.02

Table 4.5: Signal to Noise Ratio values

Since the margins obtained are bigger than the minimum value of 3 dB, for both the Energy per Bit to Noise Density and the Signal to Noise Ratio, it has been proved the receiver is able to translate the signal and to distinguish it from the noise.

4.2.2 S-Band downlink

The amount of Data needed to transferred is (4.096 $kbps$). To send this amount of data to ground, the S-Band has been chosen with a frequency 2230 MHz, in compliance with the Radio Frequency Regulation of the European Commission [39]. This presents advantages since the S-band prevents considerable impairments to electromagnetic signals due to rain, ice, and snow, it is capable of seeing beyond severe weather conditions, making it useful for civilian and military aircraft navigation. It is also useful for near as well as far-range weather observations. The Encoding method which has been adopted is the Reed Solomon Encoding in order to have only one type of encoding[38]. The S-Band antennas are isotropic [34]. These antennas are preferable since they do not require orientation and are most suitable for low frequencies. The ground station are the same used for the X-band. The amplification of the signal for the S-Band has been done using a Solid state power amplifier (SSPA), since it is lighter and performs better for the relatively small amount of data to transfer.

The system has been sized using the following variables 4.2:

P_{tot} [W]	P_{input} [W]	μ_{amp} [-]	BER_{TM} [-]	a_{enc} [-]	a_{mod} [-]
2175.6[34]	189.75	0.45[36]	1e-5[35]	1.14 [38]	28 [34]

Table 4.6: S-Band downlink variables

With the same power assumption done for the X-band and considering the efficiency of the amplifier selected from literature, the transmitted power is 85.39 W. The Minimum Energy per

Bit to Noise Density $\frac{E_b}{N_0}$ has been estrapolated from the graph, using the BER as input and looking at the Reed Solomon Encoding curve [38], and it results as 5.5 *dB*. The Real Data Rate has been obtained multiplying the data rate times the ratio between the encoding coefficient α_{enc} and α_{mod}, and it results to 166.77 *bps*. The transmitting antenna has been selected as an isotropic antenna. The gain has been considered unitary, while the gain of the receiving antenna has been found as 45.8 *dBi* from [41]. Concerning the evaluation of the losses, the following values has been obtained 4.11:

$L_{cable-rx}$ [dB]	$L_{cable-tx}$ [dB]	L_{space} [dB]	L_{point} [dB]	L_{atm} [dB]
-2[35]	-2[35]	-157.64	-0.0017	-0.037 [35]

Table 4.7: S-Band Losses evaluation

An average value has been selected for the cable losses for both receiver and transmitter. The losses associated to the distance have been evaluated assuming the maximum distance between the satellite and the Ground Station. The losses linked to the pointing of the antenna have been computed using the typical pointing error of 0.01° and a beamwidth of 0.85°. The atmospheric losses have been assessed looking at the tables from literature[35]. From the losses and the gain of the transmitting antenna, the EIRP has been computed and, consequently, the receiver power P_{rx} = -90.82 *dB*. The system noise density, calculated using a sensor temperature of 190 *K* [41], the error per bit noise density and its margin have been computed and they are reported in the following table 4.8:

N_0 [dB]	$\frac{E_b}{N_0}$ [dB]	$(\frac{E_b}{N_0})_{min}$ [dB]	$Margin$ [dB]
-205.81	92.77	5.5	87.27

Table 4.8: System noise downlink

Assuming the typical value of 78° for the Modulation Index, the Carrier Modulation Index Reduction is −23.01 *dB*, so, the Carrier Power is −113.83 *dB*. Using the same logic of the X-band analysis, the receiver bandwidth of 7.413 *MHz* has been considered. The following value of Signal To Noise Ratio have been obtained 4.9:

SNR_{car} [dB]	SNR_{min} [dB]	SNR_{margin} [dB]
23.28	20.00[42]	3.28

Table 4.9: Signal to Noise Ratio values S-band downlink

As well as the X-Band, also in this case the margins obtained are bigger than the minimum value of 3 *dB*. The conclusions are the same already explained in the previous section.

4.2.3 S-Band uplink

The process used for the uplink evaluation is similar to the one used previously, however some data are different. The system has been sized using the following variables 4.10:

$datarate$ [$kbps$]	$frequency$ [MHz]	P_{tot} [W]	μ_{amp} [-]	BER_{TC} [-]	a_{enc} [-]	a_{mod} [-]
2	2053.4	200 [34]	0.45[36]	1e-7[35]	1.14 [38]	28 [34]

Table 4.10: S-Band uplink variables

The S-Band has been chosen to obtain the same advantages explained for the S-band downlink. The Encoding method which has been adopted is the Reed Solomon Encoding in order to have only one type of encoding[38].

With the same power assumption done for the S-band and considering the efficiency of the amplifier selected from literature, the transmitted power is 200.00 W. The Energy per Bit to Noise Density $\frac{E_b}{N_0}$ has been estrapolated from the graph, using the BER as input and looking at the Reed Solomon Encoding curve [38], and it results as 6.2 dB. The Real Data Rate has been obtained multiplying the data rate times the ratio between the encoding coefficient α_{enc} and α_{mod}, and it results to 81.43 bps. The gain of the transmitting antenna has been found as 44.8 dBi from [41]. Concerning the evaluation of the losses the following values has been obtained 4.11:

$L_{cable-rx}$ [dB]	$L_{cable-tx}$ [dB]	L_{space} [dB]	L_{atm} [dB]
-2[35]	-2[35]	-156.92	-0.037 [35]

Table 4.11: S-Band uplink Losses evaluation

The assumption adopted in the computation of the losses are the same already explained in the previous chapters, as well as the method used to compute EIRP and P_{rx} and the error per bit noise density and its margin. All the values obtained are reported in the following table4.12:

P_{rx} [dB]	T_e [K]	N_0 [dB]	$\frac{E_b}{N_0}$ [dB]	$(\frac{E_b}{N_0})_{min}$ [dB]	$Margin$ [dB]
-90.88	250	-204.62	94.64	6.2	88.44

Table 4.12: System noise uplink

Assuming the typical value of 78° for the Modulation Index, the Carrier Modulation Index Reduction is -13.64 dB, so, the Carrier Power is -97.33 dB. Using the same logic of the previous analysis, the receiver bandwidth of 1000 Mhz is the higher reachable, so this value has been taken into account. The following value of Signal To Noise Ratio have been obtained 4.9:

SNR_{car} [dB]	SNR_{min} [dB]	SNR_{margin} [dB]
23.44	20.00[42]	3.44

Table 4.13: Signal to Noise Ratio values S-band uplink

As well as the other case the margins obtained are bigger than the minimum value of 3 dB. The conclusions are the same already explained in the previous section.

Chapter 5

Attitude and Orbit Control Subsystem

5.1 AOCS architecture [43]

The AOCS (Attitude and Orbit Control Subsystem) architecture of the *Metop-A* has been chosen in accord to the *"Three-axes Stabilized"* method, that lead unlimited pointing capability in any direction with the best pointing accuracy (only limited by sensors), but requiring a large power demands. Has been used this type of architecture due the high accuracy demands of the mission, because the orbit has to be *Sun-Synchronous*, but, at the same time, the -z-axis [43] of satellite has to point the Earth and the solar panels have to be point the Sun. The Attitude and Orbit Control strategy is designed to ensure an almost perfect commanding over a period of 24 hours, a good commanding over three days and a survival capability over one week without communication. In order to ensure the signal reception of the up-link AOC strategy, the datas are updated twice per day, therefore a loss of one up-link does not affect the quality of the commanding on board.[47]

To perform the attitude and orbit determination on the *Metop-A* are used these attitude sensors:

- **Digital Earth sensors:** used for the roll and pitch axes attitude determination. It use Earth-relative information combined with accurate orbital data to evaluate absolute attitude reconstruction (accuracy: 0,05-1 deg);
- **Sun sensors:** used for the yaw axis attitude determination. It use a provided Sun direction vector combined with ephemeris of the Sun to have absolute attitude reconstruction. It will not work during eclipses (accuracy: 0,005-3 deg);
- **Two-axis gyros:** used for attitude propagation during loss of external attitude reference. It provide angular rates and attitude evolution combined with external attitude reference to have absolute attitude states. Four gyros are mounted on the *Metop-A*, two of them in cold redundancy.

It has to be pointed also that in the MetOp-A are present other sensors, which are not used for the attitude:

- **Magnetometers:** Since the satellite is designed with magnetorquers it's necessary to have a precise value of the magnetic field and for this three possible choices could be made:
  1. To couple a magnetometer, in order to compute the real time Magnetic Field value.
  2. To build a computer with an accurate enough model of the Magnetic Field.

3. To communicate the Magnetic Field values each time the satellite interact with the Ground Station.

Between all of this options, for the mission studied, only the first two are really feasible, assuming to pick the easiest solution the magnetometers were considered.

- **SAS:** Coupled with the Sun Sensor is used in the safe mode.

Regarding the actuators different choices have been done:

- **Reaction Wheels:** 3 of them are necessary for the *Three-axis stabilized* architecture, and 3 have been selected, with an angular momentum of 40 $N \cdot m \cdot s$. It could be said that usually reaction wheels work with a redundant fourth wheel, in a pyramidal composition for example, in the MetOp-A mission instead are used other type of actuators to reach this safety degree.

- **Magnetorquers:** Their principal purpose is to support the reaction wheels preventing, or slowing down, the desaturation of the latter, their magnetic moment is 315 $A \cdot m^2$.

- **Thrusters:** As said in Homework 2, 16 hydrazine thrusters are assembled in the satellite, with half of them as redundant. These actuators are capable to give a torque in all the satellite principal axis, and a thrust in the $\pm$Y axis. The job of this instruments is to operate during the detumbling/slew phase, actively desaturate the reaction wheels and perform orbit manouvres when necessary.

Reaction wheels have different advantages such as: fast response, small size and mass and no fuel consumption. Also the instrument on board require high pointing precision which these actuators guarantee. Furthermore a configuration of 3 reaction wheel grants stabilization in all three direction. Magnetorquers are used to delay the saturation of reaction wheels. Since the spacecraft operates are in LEO, they give compliant value, due to the intensity of the magnetic field at such altitude, however it is not possible to control the parallel axis. In addition to orbital manoeuvres, thrusters are used to desaturate reaction wheels and to control the satellite during the safe mode. The reference frame with respect to which AOCS performances are monitored and controlled is the so-called *Spacecraft Attitude Piloting Frame* (Figure: 5.1). This is nominally parallel to the satellite frame, defined as a fixed reference frame with respect to the spacecraft body, but commanding capability is provided in order to be able to define rotations, in all three directions, of the piloting frame around the satellite frame. These rotations are uplinked in the form of the transformation matrices from the gyroscope axes to the desired piloting frame, for the two gyroscopes selected for attitude monitoring. These rotations are carried out making use of the spacecraft wheels and magneto-torquers, and not of the thrusters. This means that, if everything works as expected, they do not imply a waste of fuel and do not have an impact on the achievable re-entry times [46].

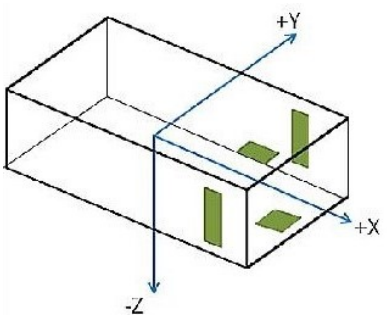

Figure 5.1: Spacecraft Attitude Piloting Frame

The overall pointing error has been defined for the *Metop-A*, according to the accuracy of sensors and actuators implemented and the requirements of the payload. APE and RPE have been found statistically from the mission *Metop-SG*, while AKE is for the studied satellite [43]. The following table 5.1 shows the error values for each axis.

Pointing Error Requirement (PER)	**Metop-A in LEO Absolute**			**Metop-A in LEO Measured**			**Precision Pointing Error for LEO**		
Error Index	APE [44]			AKE			RPE [44]		
Error Reference Axis	payload reference frame			payload reference frame			payload reference frame		
Founded Error Value	X	Y	Z	X	Y	Z	X	Y	Z
	0.9	0.9	0.9	1.22	1.74	2.97	40	40	250
Unit	mrad			mrad			mas		
Level of Confidence P_c	99.7			99.7 %			68.3 %		

Table 5.1: MetOp pointing error

5.2 AOCS Reverse sizing

5.2.1 Pointing Accuracy, Sensors and Actuators

The pointing requirements of the Metop-A have been studied considering the modes of the mission and the subsystems of the satellite.

1. **Slew mode:** the slew manoeuvre is done at the beginning of the operational life of the satellite and it is implemented with thrusters. The slew rate should be less than 0.3°/s in order to avoid payload damages. While, for the Telecom subsystem, AKE and APE should be very low because the connection with the ground station must be always satisfied. These two errors are associated to the pointing loss of the Ground Station Antenna because telemetry data are sent by the satellite with an omnidirectional antenna.

2. **Operational Mode:** in the operational mode the goal of the satellite is to collect the scientific data and to maintain the designed attitude. The payload measurements require an high Earth pointing accuracy, as well as for the Telecom subsystem, since the huge amount of data are downlinked in a short time window and it is necessary to establish rapidly the connection with the Ground Station. The knowledge error is between 0.1°-1°, which depends on the accuracy of the sensors adopted, while the performance accuracy is well below because using reaction wheels and magnetometers as control actuators is possible to reach a very precise final pointing. This high pointing precision is required by then payload since it is based on optic scanners and cameras. On the other hand, solar arrays of the electric propulsion demand less pointing accuracy since the produced power follows the cosine law and a maximum misalignment of 10° leads to a reduced effectiveness of 1.5%.

3. **Safe Mode:** the safe mode is used in emergencies if operational mode fails or is disabled. It generally uses less power or fewer components to meet minimal power and thermal needs. The main requirement of this phase is to bring the spacecraft into a Sun pointing attitude within a time compatible with the spacecraft internal electrical energy capability to guarantee power safe. For this reason, the pointing accuracy of the solar panels should be higher, in order to maximize the production of energy, while the Telecom subsystem

is still operating for the monitoring of the working conditions and must respect the same accuracy of the other modes. The payload subsystem is switched off in order to save energy and there are not any pointing requirements.

In the following table 5.2 [53], the accuracy errors are presented according to each mode and subsystem. The first value is associated to the AKE, while the second one to the APE.

Subsystem	Slew Mode	Operational Mode	Safe Mode
Propulsion	0.1°-1°, 0.1°-1°	-	0.1°-1°, 0.1°-1°
Telecom	0.1°-1°, 0.1°-1°	0.1°-1°, 0.01°-0.1°	0.1°-1°, 0.01°-0.1°
Electric	-	4°-10°	$\leq 4°$
Payload	-	0.1°-1°, 0.01°-01°	-

Table 5.2: Pointing requirements

Except during the eclipse time (ca 10-20 min), where the Sun Sensor can not be employed, all four kind sensors are operative during all the modes. The maximum affordable error due to sensors is 1°; looking at the mean error of each sensor it is possible to see that they are all less than the AKE associated to every mode. The error in the electric subsystem depends only on the Sun Sensors and Sun Acquisition Sensors, which maximum error is anyway lower than the minimum possible error. For the performance error, it is necessary to keep a very precise Earth pointing to maximize the optimal working condition of the payload. For this reason, reaction wheels and magnetorquers have been adopted. Reaction wheels have a very high accuracy but they must be desaturated through thrusters, while magnetorquers are used because, since the spacecraft is in LEO, the Earth magnetic field intensity is higher.

Regarding the positioning of the sensors:

- **Earth Digital sensors:** For these sensors two important things have to be noticed:

  1. The presence of the Sun interferes causing an increase of the errors.
  2. Earth sensors are sensitive to the elettromagnetic impulses.

  Knowing this the placement will be done consequently.

- **Sun sensors:** They have to be placed near the solar panels, since both have to be pointed toward the Sun.

Regarding the positioning of the actuators:

- **Reaction Wheels:** It's better to have the entire set built as near as possible to the center of mass and lined with the principal inertia axes because, despite the torque would be the same, the moment of inertia would differ. As the reaction wheels are not mass-less, they are part of the system, although the total mass would not change, while the mass distribution would be different. The result is that, with masses distributed broader, the same torque will result in lower angular acceleration.

- **Magnetorquers:** They are extremely sensitive to the electric instruments onboard, so, a good position would be outboard, or still inside the main body of the spacecraft with the related shielding.

5.2.2 Operational and Slew Mode, Actuators Sizing

In this mode the reaction wheels are used for the attitude control, the magnetorquers act with a continuous desaturation exploiting the magnetic field and the thrusters apply the active desaturation with pulses when the reaction wheels are no more able to provide the required angular momentum to the spacecraft [48]. The sizing has been done in order to verify the correct operation of the actuators for the orbit maintenance and for the desaturation. At first, the main disturbances have to be estimated. Knowing the dimensions of the spacecraft and its orbit, the inertia moments and the mean distance from the Earth have been computed. The inertia moments have been computed considering the main body of the spacecraft and the solar panel, assuming an generalised mass distribution (Figure: 5.2). The main variables used in the computation are reported in the following table 5.3.

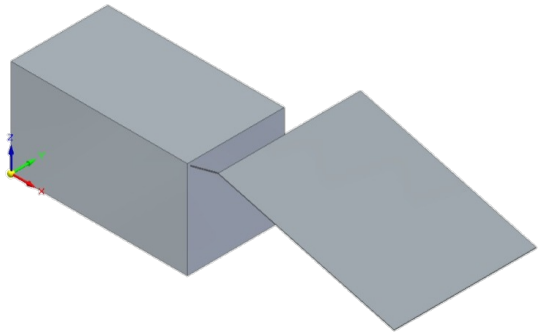

Figure 5.2: Spacecraft Model

I_{max}[kg·m^2]	I_{min}[kg·m^2]	A_{panel}[m^2]
29329.750	8017.167	32

Table 5.3: Inertia moments and Area of the Solar Panel

These data are necessary to calculate the gravity gradient disturbance, which results as the most significant disturbance. The solar radiation pressure has been estimated considering the solar panel deployed. The air drag disturbance has been obtained exploiting the exponential model to compute the air density at the orbit altitude, knowing the velocity of the spacecraft and its dimensions. At the end, all these obtained disturbances lead to a total disturbance torque equal to $9 \cdot 10^{-}3\ N \cdot m$. The computed disturbances have been compared to the effective one, detected in the real mission [49], which are expressed in the following table 5.4:

T_d[N·m]	T_m[N·m]	T_{gg}[N·m]	T_{SRP}[N·m]	T_{tot}[N·m]
$2.8 \cdot 10^{-4}$	$2 \cdot 10^{-4}$	$8 \cdot 10^{-3}$	$2 \cdot 10^{-3}$	$10 \cdot 10^{-3}$

Table 5.4: Real measured disturbances

Knowing the amount of the total disturbance torque for one orbit and substracting to it the control torque provided by the magnetorquers, multiplying this value times the period of the orbit, the value of the angular momentum to provide to the spacecraft per orbit has been obtained. Comparing this value to the maximum amount of angular momentum that the reaction wheels are able to generate, the number of orbits that have to elapse between each

desaturation has been found, and it resulted as $n_{orbits} = 8.23$. The control torque provided by the magentorquers has been computed underestimating the value of the magnetic field along the orbit (to use a more conservative approach), and knowing the value of the magnetic dipole that the magnetorquers can generate. Since the thrusters are in charge of the active desaturation, the mass of propellant required to desaturate has been found. Imposing a reasonable time needed for the desaturation equal to 5 s, the thrust that the thrusters have to provide resulted as 1.1765 N, which is feasible since the maximum torque that they can provide is 23.5 N and since they work with monopropellant. The mass of propellant required to desaturate one single reaction wheel has been computed, and this value has been multiplied times the total number of reaction wheels (3) and to the total duration of the mission (5 *years*). The total mass of propellant for the desaturation resulted equal to 25.69 *kg*. The mass of propellant required to apply all the desired slew manoeuvres during the operational life of the satellite has been recovered, since the thrusters are the actuators chosen to provide the torque for the slew manoeuvre [50]. The thrusters implemented in the satellite are able to generate a minimum thrust of 8 N and to work through pulses [48]. However, in order to obtain a preliminary sizing, the thrust provided has been assumed to be constant and continue over time; this assumption led to a minimum thrust lower than the nominal one. The satellite angular velocity during the slew manoeuvre has been selected as $\dot{\theta} = 0.3°/s$ from [52], and the maximum angle considered for the slew has been chosen as $\theta = 270°$ because also the anti-slew manoeuvre has been taken into account. From these variables has been possible to compute the minimum time needed for the manoeuvre as well as the minimum thrust requested. At the end, the mass of propellant for one slew (and anti-slew) manoeuvre resulted as 0.1795 *kg*, so the total mass for the entire life time of the mission, considering one slew and anti-slew every 18 months, corresponds to 0.7178 *kg*.

5.2.3 Safe Mode, Actuators Sizing

In this mode the thrusters work in order to control the attitude of the spacecraft instead of the reaction wheels [48]. The recovery time can be anywhere from a few hours to days or weeks depending on the difficulty in reestablishing communications, conditions found on the spacecraft, distance to the spacecraft and the nature of the mission, so, in order to use a conservative approach, it has been considered a maximum duration of two weeks for this mode [47]. It has been then possible to compute the amount of mass of propellant required for this mode. The thrusters can be used in attitude control through impulses, however, in order to obtain a preliminary sizing, the thrust provided has been assumed as constant and continue over time, as weel as it has been done in the previous section. From the performances of the thrusters [51], considering the maximum duration of the safe mode, and taking into account that the thrusters have to counteract the total disturbance torque, the total mass of propellant needed to control the spacecraft using the thrusters has been obtained and it resulted as $m_{prop-safe} = 4.825$ *kg*.

Chapter 6

Thermal Control Subsystem

6.1 TCS architecture

The TCS (Thermal Control Subsystem) of the Payload Module on the Metop-A has been designed taking in account the temperature requirement for the instruments and their heat load. It is composed by:

- **Multi-Layer-Insulation (MLI):** insulate the spacecraft with multiple layers of reflective materials designed to minimize the incoming heat flux form outer sources;
- **Flexible Second Surface Mirror Radiators:** promote heat dissipation by IR (Infrared) radiation by deploying a heat dissipation surface;
- **Thermal Doublers:** spread the heat of high dissipating units;
- **Black Paint:** maximise the radiative exchanges on inner side of PLM panels;
- **Heaters system:** made of an hardware part, that control heaters use thermostats and maintain minimum non-operating temperatures, connecting the Payload Module Computer (PMC), the Thermal Control Unit (TCU), the Power Distribution Unit (PDU) and the Power Control Unit (PCU), and a software part, that control the PMC on the basis of thermistor readings and defined temperature limits;
- **Thermistors:** monitor the temperature of the different interesting part of PLM (Payload Module);

Most instruments have their own thermal control and are thermally de-coupled from the PLM structure. The TCS of the Service Module is made by similar techniques used for the PLM, through which is possible to study:

- **Batteries:** mounted on a radiator plate and enclosed in a compartment thermally insulated from the rest of the spacecraft;
- **Propulsion subsystem:** insulated from spacecraft, it ues MLI and heaters when needed;
- **Solar Panel:** using passive thermal control components (like MLI and thermal finishes) and active thermal control in form of heaters, which are used only in the LEOP, after the separation of the spacecraft from the launcher and up to the complete deployment of the solar arrays;

The frame structure configuration has been designed to guarantee the least interference possible, for the instruments field of view, and also to minimize the shadowing of instruments radiators. This frame allows the installation of the instrument in its nominal configuration and it allows its rotation by 65 degrees before mounting it back to the PLM. The accommodation of a large complement of instruments has been a significant design driver for the overall PLM configuration, with many constraints given by the instrument fields of view, antenna patterns, and thermal radiators.

Despite the different design and configuration selected for Payload Module and Service Module, the functioning of the whole thermal control subsystem is runned by the central on-board software in the Service Module. The interfaces between the two modules have been studied in order to minimize their number as much as possible: mechanical interfaces consist of the connection between the modules, electrical interfaces are limited to power and OBDH bus, data exchanges use telemetry and telecomand packets. The interfaces between the two modules also guarantee a very limited thermal exchange transferred from PLM to SM and viceversa.

The goal of the TCS is to keep the components of the satellite, for both Service and Payload module, inside their constraining operating temperature ranges. Moreover, the external heat sources during the mission has been evaluated. The choices for the TCS have been made starting from this analysis. The infrared heat flux is the highest one, for this reason, radiators have been chosen because they promote heat dissipation though IR radiation by deploying a heat dissipation surface. Furthermore, Silver-Teflon coating is useful to minimize the incoming heat flux, while Multi-Layer-Insulation is able to contain inside the heat produced by the spacecraft. The following table 6.1 shows the operating temperature ranges of all the main components of the spacecraft. The maximum allowable temperature is imposed by Lithium batteries, while the minimum one is imposed by the hydrazine tanks. This restraining temperature range drives the sizing of radiators surface and heaters power.

Component	Operational Temperature $[^{\circ}C]$
Reaction wheels	from -10 to $+40$
Magnetorquers	from -25 to $+70$ [59]
Sun sensors	from -45 to $+80$ [60]
Digital Earth sensors	from -25 to $+70$ [61]
Gyroscopes	from 0 to $+40$
Ni-Cd Battery	from $+10$ to $+30$
Solar panels	from -165 to $+130$
Hydrazine Tanks	from $+15$ to $+50$ [62]
OBC	from -5 to $+40$
Data Processing Unit	from -20 to $+50$
Antennas	from -100 to $+100$

Table 6.1: Operating temperature ranges

The minimum operational temperature is $T_{min} = +15\,\text{deg}$ and the maximum one is $T_{max} = +30\,\text{deg}$. In order to size properly the subsystem, a margin of $-5\,\text{deg}$ has been used in the hot case, while a margin of $+9\,\text{deg}$ has been used in the cold case to not overcome the hot case temperature.

6.2 TCS reverse sizing

The reverse sizing of the thermal control system has been done using the mono-node assumption, in which the dimensions of the spacecraft with the solar panel non deployed has been taken into account, since it can be considered as thermal independent with respect to the rest of the spacecraft 6.1.

Figure 6.1: Metop-A

A further mono-node analysis of the solar panel has been done in order to verify that the temperatures reached in both cold and hot case fall within the safe range. The area of the equivalent sphere of the main body resulted as $A = 107.44\ m^2$, and the radius as $r_{s/c} = 2.924\ m$. The first thermal heat sources which has been considered is the solar flux, which corresponds to the solar flux at the distance of 1 AU since the orbit of the mission is around the Earth. The albedo flux has been computed assuming an albedo factor as the highest of the typical range $(0.31 \div 0.39)$[64] as well as the angle between the spacecraft and the planet, which has been considered as $0°$ in order to be conservative. In the computation of the infrared flux, a surface temperature of 298 K and an infrared emissivity of $\epsilon = 0.90$ have been used [57]. The same evaluation has been done for the solar panel, with an area of 30.2 m^2. Its absorbptivity and emissivity have been picked as $\alpha_{panel} = 0.9$ and $\epsilon_{panel} = 0.7$ from [63]. The power used in the computation has been assumed as null since the amount of power involved is smaller with respect to the amount of power used in the main body computation, for both cold and hot cases. The heat fluxes and the temperatures reached obtained are reported in the following table 6.2.

$Q_{sun}[W]$	$Q_{albedo-h}[W]$	$Q_{IR-h}[W]$	$Q_{IR-c}[W]$	$T_{hot}[K]$	$T_{cold}[K]$
$9.2922 \cdot 10^3$	$3.0611 \cdot 10^3$	$2.5664 \cdot 10^3$	$2.4992 \cdot 10^3$	334.02	213.69

Table 6.2: Solar Panel Fluxes and Temperatures

As it can be seen from the table 6.2, the temperatures reached from the solar panel fall within the allowable range, so there is no need to implement radiators or heaters on it.

6.2.1 Hot Case

The hot case is associated to the operational phase of the spacecraft, when all the modules are operative and the electric power is provided by the solar arrays. The $P_{int} = 1045\ W$ used in the

computation has been retrieved considering half of the difference between the maximum total power of 3890 W from the solar panel and the power consumed by the instruments, payload and service module of 1810 W. The remaining half is dissipated by the instrument module [54]. The spacecraft is assumed to be hitted by all the possible fluxes and its position is at the pericentre (in which the albedo and the infrared fluxes have the maximum value). The maximum powers computed are reported in the following table 6.3.

$Q_{sun}[W]$	Q_{albedo}[W]	$Q_{IR}[W]$
$1.8366 \cdot 10^3$	605.01	118.69

Table 6.3: Heat Fluxes in the Hot Case

The powers reported above have been computed starting from the heat fluxes of the previous section. For the Sun power, the cross sectional area and the solar absorptivity of the spacecraft have been considered in the computation as $A_{cross} = 26.86\ m^2$ and $\alpha_{coat} = 0.05$ from [58]. The albedo power has been calculated using a diffusion factor of the planet as 1 to be conservative, a planet-spacecraft view factor as $F_{pl-sc} = 0.2676$ computed considering the radius of the Earth, the spacecraft at the pericentre and the same α_{coat}. The same F_{pl-sc} has been used to compute the infrared power. The emissivity of the spacecraft has been assumed as 0.013 from [65].

In order to size the area of the radiators, the temperature of the spacecraft has been imposed as the maximum temperature acceptable, which comes from the batteries, considering a margin of $-5K$. The temperature reached by the spacecraft is 461.9 K, which is above the maximum temperature of 298 K; for this reason, radiators must be implemented. The area of the radiators which guarantees the correct operation of the spacecraft has been obtained and it resulted as $A_{rad} = 7.69\ m^2$, using an emissivity of the radiators of $\epsilon_{rad} = 0.88$ [64]. The percentage of the area covered by the radiators resulted as 7.16% of the total area of the mono-node sphere.

6.2.2 Cold Case

The cold case occurs during the Early-orbit Operations Phase and the eclipse phases, when the solar panel is not already deployed and the electric power is provided by the batteries. The power used in the cold case computation is the same used in the hot case scenario, reduced to $P_{eclipse} = 800\ W$, which is a proper amount since the power to dissipate in the eclipse phase is smaller with respect to the one in the operational phase. Since this cold condition occurs during the eclipse phase, the albedo and the solar fluxes have not been considered; only the infrared flux has been taken into account, which has been computed in the worst case (spacecraft at the apocentre), and it resulted as $Q_{IR} = 115\ W$. The same area and a $F_{pl-sc} = 0.2631$ have been used. The temperature reached considering the presence of the radiators is 211.55 K, which is less than the minimum temperature imposed by the hydrazine tanks considering a margin of $+9\ K$. This led to the need to implement heaters onboard, which has been accordingly sized. Using the same emissivity of the spacecraft, and imposing a temperature of 297 K, the heat power resulted as $Q_{heaters} = 2.64 \cdot 10^3\ W$, which is higher than the actual power addressed to this system. The reasons that justify this result are related to a previous overestimation of the radiators surface in the hot case scenario, and to an higher value of the internal power involved in the eclipse phase, during which some components should be considered as switched off.

Chapter 7

Electric Power Subysystem

7.1 EPS architecture

The EPS (Electric Power Subsystem) of the Metop-A consists of an eight-panel solar array, supported by five batteries that store energy and a dedicated power conditioning strategy. The SA (Solar Array) on the Metop-A is a single wing, flat pack design made of eight hinged rigid silicon solar cells panels (each 1 m x 5 m)[69], equipped with Back Surface Reflectors (BSR) type solar cells, in order to reduce the operating temperature by decreasing the absorbance. The unusual configuration of the SA (Figure: 7.1) has been chosen to increase the maximum power generation, having the right angles to the Sun as much as possible; indeed, due to the polar orbit of the satellite, the Sun always shines from the left side, with an almost constant angle of about 40 degrees (*wrt* the SC body). This configuration guarantees a better angle and can also rotate around the east-west axis of 20° to compensate for the moving Sun. The responsible for this rotation is the SADM (Solar Array Drive Mechanism), which has been mounted on the spacecraft side of the interface, using an equipped motor to perform that rotation, and some instruments to keep track of the position, the temperatures and the state of the SA. It can also be said that the placement of the solar array is to avoid partial shadowing of the satellite bus, which would create mechanical stresses from the thermal gradients and disrupt its infrared sensing instruments. In this way, the maximum generated power is 3.890 kW (EOL), and the average power over one orbit is 2.210 kW (EOL) [66].

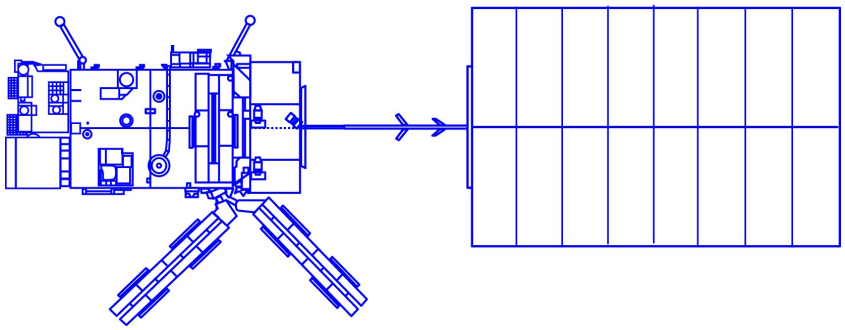

Figure 7.1: Solar Array Deployed

In order to support the mission during the Launch and Early Orbit Phase (LEOP), the eclipse orbit phase and the temporary power peak during the sunlight phase, a set of five 40 Ah Nickel-Cadmium batteries has been mounted on the Metop-A. The batteries are located

on the bottom of the service module, equispaced on the support plate (Figure:7.2). Since the top part of the service module contains the four propellant tanks, at the interface between the *PLM* and the *SVM* itself, the batteries have been located far from the tanks and the *PLM*, in order to avoid heat exchange from the batteries to the tanks and to the *PLM*.

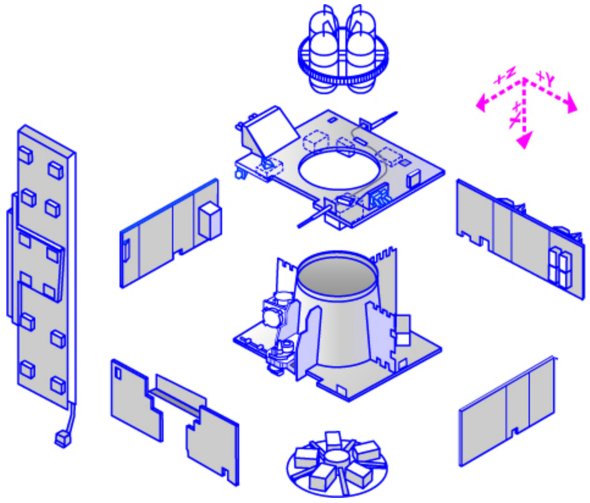

Figure 7.2: Exploded View of Service Module with Propulsion

The Power Regulation & Control s/s is composed of a dedicated unit (RSJD) (Figure: 7.3) that is in charge of the:

- balancing the SA power income;
- regulation of the power requirements for spacecraft and battery recharging;
- managing the thermal control of the batteries;
- granting the satellite management in case of failure conditions with the switch-off of connections;

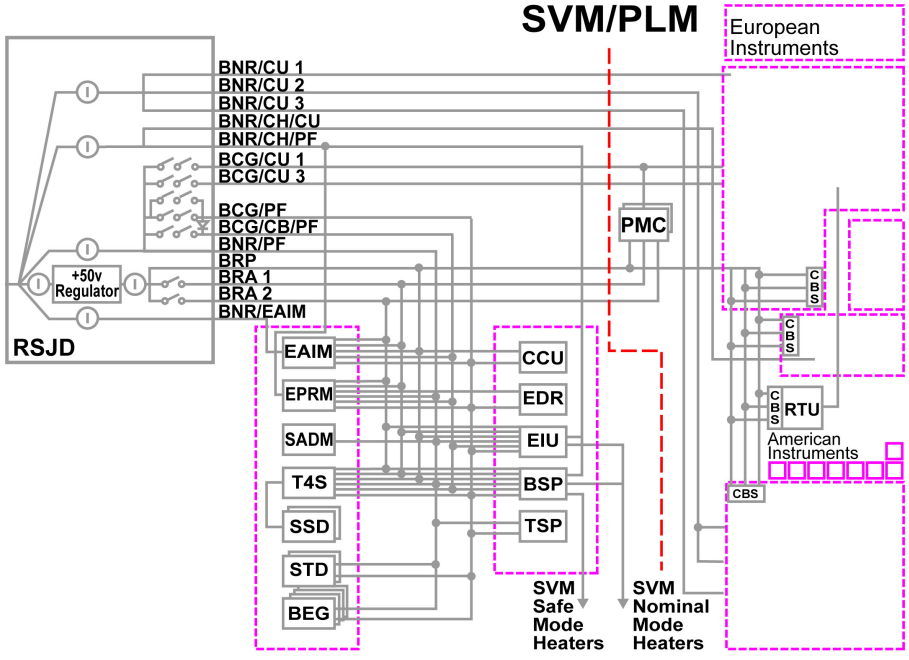

Figure 7.3: RSJD Power Distribution

That dedicated unit (RSJD) is composed by:

- **Permanent Unregulated Bus**: to distribute power to the Service Module (SVM) and Payload Module (PLM) units (22-37.5 V);
- **Permanent 50 V Regulated Power Bus**: to distribute power for SVM low-level electronic functions and bus couplers;
- **Switched 50 V Regulated Power Buses**: to switch off SVM and Payload Module Controller bus couplers;

The unregulated bus has been implemented since it has a design that delivers the expected output at a given current, not always reflecting the actual voltage output. These power supplies are simple, low-cost options that have the major disadvantage of providing uneven voltage. The slight changes in voltage output do not matter for some applications, resulting cheaper with respect to other alternatives. On the other hand, the regulated power bus has also been implemented, which has all the same parts as the unregulated one with the addition of a voltage regulator. This regulated power bus ensures the output delivered is smooth and unchanging, regardless of draw or input [71]. It has also been provided a personal 28 V Power Control Unit (PCU) for the American instruments, located in the Payload Module. Starting from the average power consumption of the satellite of 1813 W, it has been used a margin of 20% to size the power, since the Metop-A is a newly designed and developed product. The resulting total power of 2175.6 W has been reduced by the power consumed by the instrument (910.6 W), resulting in 1265 W. The power for each sub-system has been assigned starting from this and considering the power distribution for a meteorological satellite [73]. The maximum consumption per each s/s have been presented in the table underneath 7.17.2, expressed in W, where they have been analyzed for each mode and sub-system.

Subsystem	**LEOP**	**SIOV**	**Commissioning**	**De-orbiting phase**
	Mode 1	**Mode 1**	**Mode 1**	**Mode 1**
Instruments	Off	215	210	Off
Data handling	Off	164.45	164.45	Off
Telecom	189.75	189.75	189.75	189.75
Propulsion	~ 0	~ 0	~ 0	~ 0
Attitude actuators	240.35	Off	240.35	240.35
Electric power	63.25	63.25	63.25	63.25
Thermal control	607.2	607.2	607.2	Off
Total	1100.55	1239.65	1475	493.35

Table 7.1: Power budget

Subsystem	Routine Operation			EOL
	Slew Mode	Operational Mode	Safe Mode	Mode 1
Instruments	910,6	910,6	Off	Off
Data handling	164.45	164.45	Off	Off
Telecom	189.75	189.75	189.75	Off
Propulsion	~ 0	~ 0	~ 0	Off
Attitude actuators	Off	240.35	240.35	Off
Electric power	63.25	63.25	63.25	Off
Thermal control	607.2	607.2	607.2	Off
Total	1935.25	2175.6	1100.55	0

Table 7.2: Power budget

In the LEOP phase, the instruments are not working yet, while every sub-system is operative, apart from the data handling. During the SIOV phase, the instruments are switched on only one by one, therefore the power request for the maximum consuming instrument has been used for the sizing; every s/s is operative except for the attitude actuators. In the commissioning phase the only active instrument is the IASI, in order to collect data to improve its performances; every subsystem is operative. The Routine Operation phase is divided into three modes (that will be listed below in no particular order). The first is the slew mode, where everything is working, including the instruments, apart from the attitude actuators. The second is the Operational mode, in which all the s/s and the instruments are operative. In the safe mode, the last mode of the routine operation, the instrument and data handling are not in use, while everything else is. The next phase is the De-orbiting phase, throughout which the instruments are off, such as the data handling and the thermal control; the other subsystems are working. During the final phase of the satellite, it was necessary to completely deactivate the spacecraft.

7.2 EPS reverse sizing

7.2.1 Primary Source

The solar panel, folded during launch, has been considered with a total area of 40 m^2 and a total mass of 255 kg[69]; it is made of Silicon-based solar cells. The sizing of the solar array has been done using the parameters expressed in the following table 7.3:

T_d [s]	T_e [s]	X_d [-]	X_e [-]	P_{SA} [W]	I_0 $[\frac{W}{m^2}]$	T_{life} [y]
4040	2020	0.8	0.6	3828[67]	1361	5

Table 7.3: Solar Array Parameters

For a more conservative approach the beginning-of-life (BOL) efficiency ϵ_{BOL} and the Inherent Degradation I_D have been considered as small as possible, the degradation per year dpy, instead, has been chosen as a mean value.

With this data, the SA specific power, at BOL, has been computed, and exploiting the lifetime degradation evaluated with the dpy and the T_{life}, the SA specific power produced at EOL has been obtained. Then the area of the solar panel has been evaluated. Assuming a mean thickness and density, for the Si solar arrays of respectively $5\ cm$ and 75 $\frac{kg}{m^3}$ also the total

ϵ_{BOL} [-]	I_D [-]	dpy [-]
0.20	0.49	0.028

Table 7.4: EPS coefficients

mass of the primary energy source has been achieved. All the results have been reported in the table 7.5:

$P_{BOL}[\frac{W}{m^2}]$	L_{life} [-]	$P_{EOL}[\frac{W}{m^2}]$	$A_{SA}[m^2]$	$m_{SA}[kg]$
125.33	0.8676	108.74	35	131

Table 7.5: Solar Array Results

It has to be noticed that the computed area and the real one are almost the same. The slight difference could be explained by thinking of a more conservative approach adopted in the real case. The difference between the obtained mass and the real one is instead considerable, but the real one depends on both the thickness and the mean density of the SA, which have been assumed. It could be possible to arrange those values and obtain a more reliable mass, but considering the preliminary sizing the results have been kept in this way.

7.2.2 Secondary Source

At first, the Depth of Discharge, DOD, has been obtained from the graph 7.4, considering a life of 2000 cycles[72] of the Ni-Cd batteries.

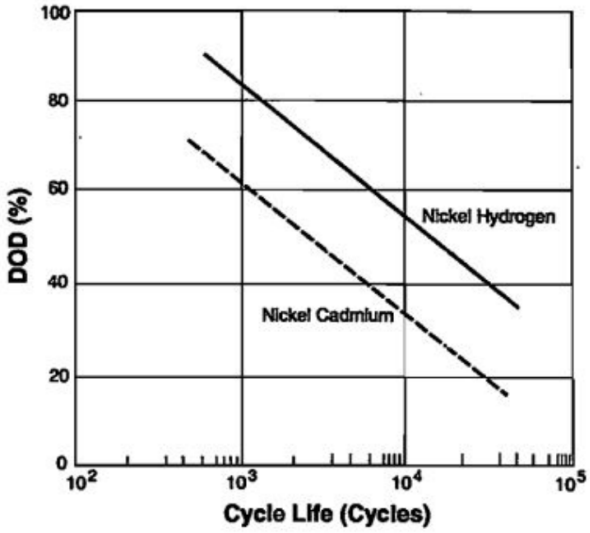

Figure 7.4: : DOD with respect to the battery cycles

The specific density, specific energy and voltage have been extrapolated by looking at the data of *Ni-Cd* batteries and they are reported in the following table 7.6.

$E_s[\frac{Wh}{kg}]$	$E_d[\frac{Wh}{dm^3}]$ [-]	$V_{cell}[V]$
40	90	1.35

Table 7.6: Batteries properties

The required capacity has been computed knowing: the previous values, the eclipse time and mean power, which has been overestimated; the line efficiency has also been taken into account. The capacity resulted in $C = 677.82\ Wh$. From this variable, exploiting specific energy and energy density, mass and volume of the batteries have been computed, and they resulted in $m_{batt} = 16.95\ kg$ and $V_{batt} = 7.53\ dm^3$. The effective capacity of each battery has been calculated overestimating its value, using the minimum system voltage from the minimum voltage of the permanent unregulated bus, resulting in $C_{fin} = 30.81\ Ah$, which is a reasonable value, compliant with the actual one.

In order to obtain a refined battery sizing, the actual system voltage has been retrieved, considering the voltage of the single battery and the voltage of the system. The real voltage resulted in $V_{real} = 22.95\ V$, with $N_{series} = 17$.

Considering a packaging efficiency ($\mu = 0.8$), and the single cell capacity, the number of strings in parallel has been obtained as $N_{parallel} = 8$, so the actual battery system capacity resulted as $C_{real} = 734.4\ Wh$.

Chapter 8

Configuration Analysis and On Board Data Handling

8.1 MetOp-A Configuration Analysis

The MetOp-A configuration 8.2 has been designed according to all the technical requirements of the Payload Module and the Service Module. While, the dimension of the satellite in its packed configuration is imposed by the available envelope of the launcher, as can be seen by the figure8.1. MetOp-A has been launched by the Soyuz-ST and packed in the fourth stage called Fregat. It works as the adopter for the satellite and performs the last orbit manoeuvres for the injection orbit. With a diameter of 4.1 m and an height of 11.4 m[75] it fullfills completely the geometry requirements of the packed configuration since the satellite has a dimension of 2.5x2.5x6.3 m.

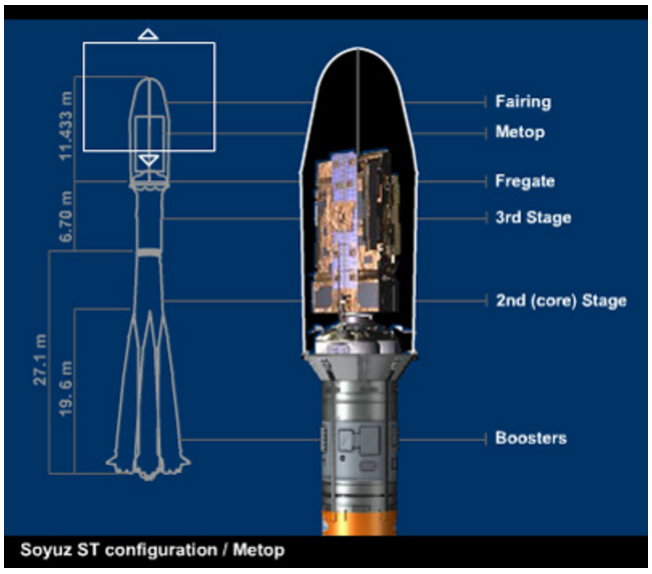

Figure 8.1: Packed configuration

8.1.1 External Components

- **Thrusters**: Two branches of eight thrusters, which allow the generation of torque in all three axis and of propulsion in the ±Y axis. They are mostly located on the Y axis and other two point toward the +X,+Z direction.
- **Solar Array**: Unusual disposition, which guarantees the maximum power generation. It

can also be rotated around the east-west axis to compensate the moving of the Sun. The solar array, once deployed, incorporates its own thermal control system, utilizing passive measures such as Multi-Layer Insulation (MLI) and appropriate thermal finishes. Active thermal control, employing heaters, is only implemented during the period following the separation of the spacecraft from the launcher until the solar array deployment is completed.

- **X-Band Antenna**: mounted on the external panel, located on the -Z face, pointing to the Earth.
- **S-Band Antenna**: located on the external panel, always pointing to the Earth (-Z direction).
- **External Configuration of the Scientific Payload Module**: it is mainly driven by the fields of view and performances of instruments, sensors, radiators and antennas, as well as the available volume under launcher fairings.

8.1.2 Internal Components

- **Internal Configuration of the Scientific Payload**: it has been designed in order to provide a sufficient radiator area for heat dissipation of internal units through passive thermal control. A failure propagation to other instruments/subsystems in case of unsuccessful antenna deployment has been taken into account. Other drivers in the configuration design have been the optimal length for loss-sensitive cabling like antenna-receiver connections and the optimal harness routing in conjunction with modular assembly flexibility. Most of the instruments are positioned towards Earth, along the -Z direction, except for GRAS, which, as it needs to communicate with other orbiting satellites, is placed along the -Y axis, as well as the GOME, which is mounted to the flight direction side of the MetOp satellite and is nadir viewing.
- **Heaters and Radiators**: the position of the radiators is driven by the local time of the ascending node, or LTAN [78]. Radiator dissipating units are installed on the side and floor panels. Multi-Layer-Insulation (MLI) blankets cover all the other faces of the main body to minimise the heat flow. Internally the panel and the electronics units are black painted to maximise the radiative exchanges. The LTAN equal to 21:30 for the MetOp-A implies the minimum thermal energy requirement from the heaters because the shadowing zone is low [79]. They are placed near the propellant tanks in order to keep constant the required storage temperature, near the instruments module, in the -Z face, to maintain the temperature within the limits.
- **Propellant Tanks**: they are positioned on a alluminum alloy plate, which interfaces between the PLM and the SVM central structure. Separated from the batteries in order to avoid heat exchange. Both the tanks and piping are temperature controlled using MLI and heaters. They are symmetric avoiding the influence on the centre of mass and are placed along the X axis.
- **Battery pack**: mounted on a radiator plate and enclosed in a compartment, which is thermally insulated from the rest of the spacecraft. The battery pack is positioned near the control electronics in order to avoid a large amount of cable losses.
- **Sun Sensor**: it provides the angle measurment along the yam axis (Z-axis) and its Field of View (FOV) is a slit normal to the radial direction with semi-angle of 21 degrees and

a off-pointing (with respect to the orbital velocity) of 36 degrees toward port-board (to be aligned with the mean Sun nominal direction for nominal LTDN of 9:30) [79]. For this reason it is allinaed with the +X axis.

- **Earth Sensor**: the digital Earth sensor measure the angular deviation along the pitch and roll axis, it is placed along the +Z axis to scan continously the Earth.
- **Reaction Wheels**: positioned along the three main axes to guarantee the stability of the spacecraft.
- **Magnetorquers**: placed far from the main body in order to reduce the influence of the internal residual dipole of the spacecraft.

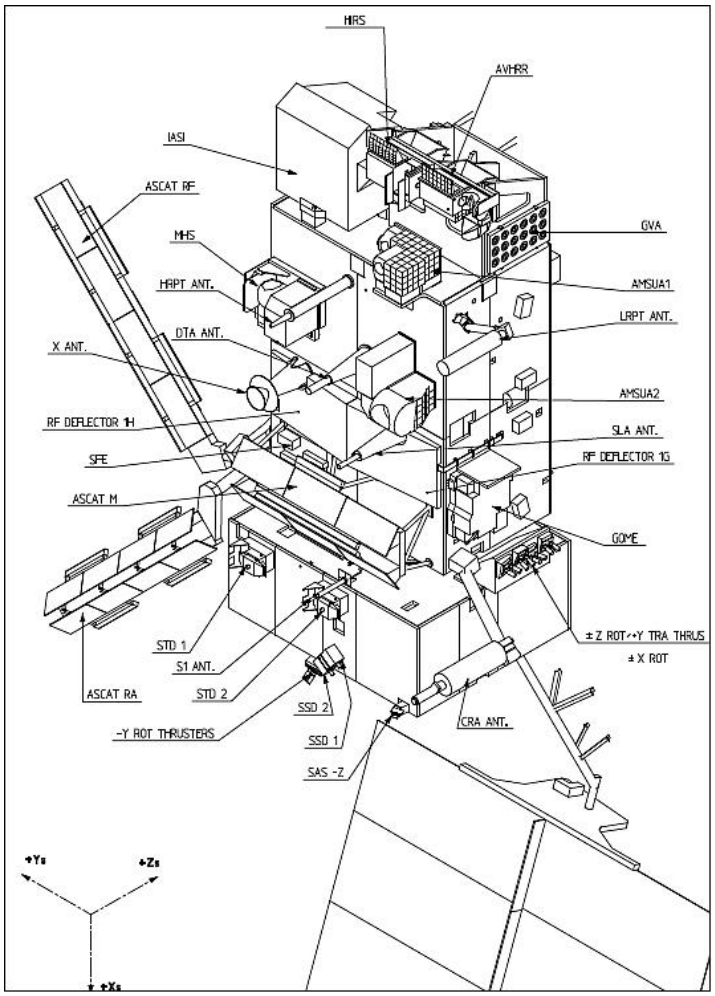

Figure 8.2: MetOp-A Configuration

8.2 On-Board Data Handling

8.2.1 OBDH architecture [76]

The On Board Data Handling (OBDH) architecture on the Metop-A is decentralized, meaning that Payload Module (PLM) and Service Module (SVM) have their own computer, and is connected by ESA Standard On-Board Data Handling (OBDH) data buses. For the OBDH s/s the CCSDS protocols has been employed. In the Payload Module (PLM), that has been

controlled by the Payload Module Computer (PCM), a dedicated NIU (NOAA Interface Unit) has been used, in order to adapt the NOAA (National Oceanic and Atmospheric Administration) interfaces with European standards. The NIU performs command and control through a dedicated Instrument Control Unit (ICU) and collects measurement data through a DSP (Digital Signal Processor). The NOAA-provided instruments (AVHRR/3, HIRS/4, AMSU-A, and SEM-2) and the selected EUMETSAT-provided instruments are encrypted by the FMU (Formatting and Multiplexing Unit) with an encryption capability selected in order to ensure commercial and data-denial needs. The European instruments (IASI, ASCAT, GOME-2, ASCAT) have been directly connected with the PCU, besides the Microwave Humidity Sounder (MHS) which uses the MPU (MHS Protocol Conversion Unit). The redundancy of two Payload Module Computer has been selected to manage eventual failures. The PLM (Payload Module) command and control functions have been performed through:

- PMC (Payload Module Computer)
- CBS (Standard Bus Couplers)
- RTU (Remote Terminal Units)
- DBU (Digital Bus Units)
- RBI (Standard Remote Bus Interface ASICs)
- ICU (Intelligent Control Units)

Due to the large data from sensors and the huge dimension of s/c, an RTU has been designed to offloads the Payload Module Computer, assigning it responsibilities of:

- gathering the analogue and digital telemetry from sensors and units and sending it at PMC;
- sending the determined controls from PMC to instruments and PDU;
- controlling the Power Control Unit (PCU);

The scheme of the PLM command and control architecture has been presented in the figure 8.3.

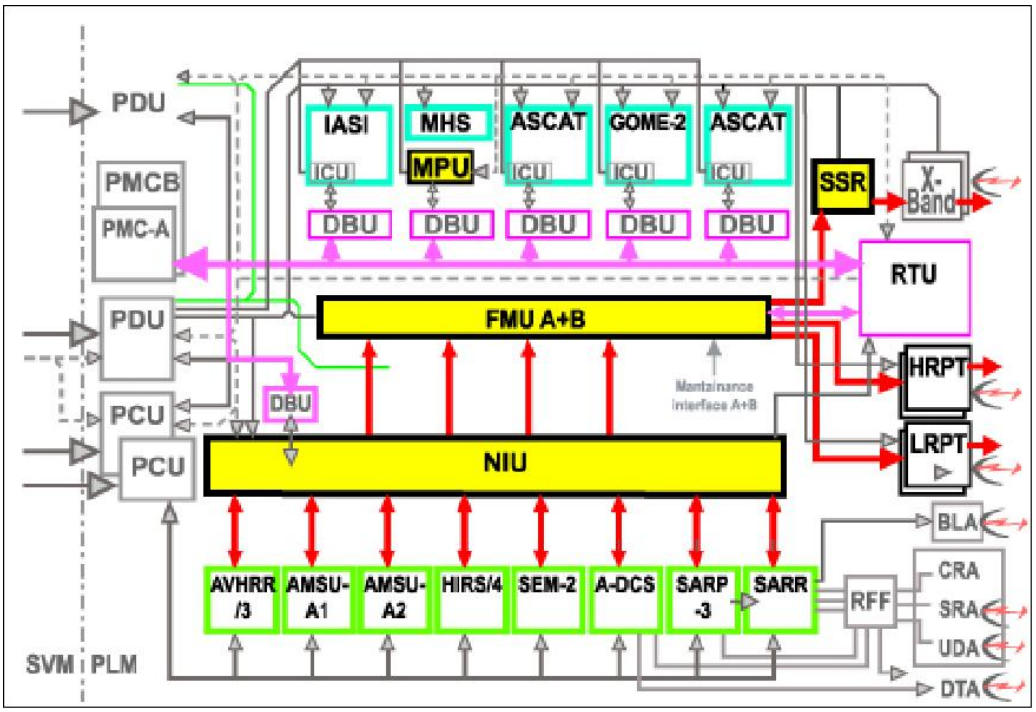

Figure 8.3: PLM data acquisition

As could be notable also from the figure 8.3, the PLM architecture is *Federated Bus* with buses for command response protocols and which rely on traffic arbitration. That configuration has been chosen due to the high number of instruments that need a deterministic and time reduced transmission, with also the benefit of increased troubleshooting and reliability, nonetheless comporting the necessity of specific interfaces (physical and electrical).

The Service Module command and control function has been designed relying on the SPOT MK3 bus. The data management has been done by the Central Communication Unit (CCU), with a MA31750 microprocessor with two redundant memory modules of 224 Kwords, performing the data exchange with the OBDH bus, bus couplers and on-board time generation and synchronization. In the SVM are also present:

- **Decoding and reconfiguration unit (EDR)**: used with the S-band transponder, to carry out the telecommand receipted and to give to the Command Pulse Direct Unit (CPDU) telecommands and to the CCU supervision.
- **Housekeeping and pyrotechnics unit (BSP)**: in charge of generation of pyrotechnic commands, housekeeping of some SVM units, temperature measurements and conseguent actuation of heaters for the SVM;
- **Electrical Interface Unit (EIU)**: in charge of the release and deployment of the solar array and the TM\TC (Telemetry and Telecommand) of these part;

8.2.2 OBDH Reverse Sizing

The sizing of the OBDH has been done considering the systems present onboard and using the typical values of code, data, typical kips, typical frequency and acquisition frequency taken from [80][81]. They have been used to compute the *KIPS* for each component, which have been presented in the table 8.1:

Components	Number	Acquisition frequency	KIPS
ADCS			
Reaction wheel	3	1	2.5
Thruster	8	1	0.6
IMU	2	10	9
Sun Sensor	2	1	1
Earth Sensor	1	10	12
Magnetometer	3	10	5
Magnetorquer	2	10	5
Kinematic integration	1	10	15
Error determination	1	10	12
Attitude determination	1	10	150
Attitude control	1	10	60
Complex ephemeris	1	1	8
Orbit propagation	1	1	20
PS			
Tank	4	-	-
Tank Control Valve	16	0.1	3.0
Tank Pressure Sensor	16	0.1	3.0
EPS			
Solar Panel	1	-	-
Batteries	5	-	-
Cable & Hardness	1	-	-
Power Voltage Control	1	0.1	0.5
Power Current Control	1	0.1	0.5
TCS			
Thermal Control	1	0.1	3.0
TT&C			
X-Band	1	-	-
S-Band	2	-	-
Transponder 2 (Uplink)	3	10.0	7.0
Transponder 2 (Downlink)	3	10.0	3.0
System			
IØDevice Handlers	1	1.0	10.0
Test and Diagnostic	1	1.0	5.0
Math Utilities	1	1.0	5.0
Executive	1	10.0	60.0
Run Time Kernel	1	10.0	60.0
Complex Autonomy	1	10.0	20.0
Fault Detection	1	1.0	3.0
Fault Correction	1	10.0	10.0

Table 8.1: KIPS

The total throughput have been computed considering the kips and the number of each component, the total code and data have been computed considering the code and data for each component. The results have been presented in the table underneath 8.4, considering a coefficient of 1 for a more conservative approach:

	ADCS	EPS	PS	TCS	TT&C	Payload	OS	TOT
Communications								
throughput	334,3	1	0	3	30	0	173	541,3
margined	1671,5	5	0	15	150	0	865	2706,5
Code	73000	2400	0	800	6000	0	36400	118600
margined	365000	12000	0	4000	30000	0	182000	593000
Data	21300	1000	0	1500	19500	0	28300	71600
margined	106500	5000	0	7500	97500	0	141500	358000
Manouvering								
throughput	334,3	1	96	3	0	0	173	607,3
margined	1671,5	5	480	15	0	0	865	3036,5
Code	73000	2400	25600	800	0	0	36400	138200
margined	365000	12000	128000	4000	0	0	182000	691000
Data	21300	1000	48000	1500	0	0	28300	100100
margined	106500	5000	240000	7500	0	0	141500	500500

Figure 8.4: Results table

The ROM has been obtained by summing the code of each s/s and has been converted into *byte* considering a conversion ratio of 16 *bit/words* equal to the microprocessor mounted, the RAM has been obtained considering both the data and the code, with the same conversion ratio used for the ROM. They have been presented in the table below 8.5.

TOT Code [kb]	TOT Data [kb]	TOT Tp [KIPS]	TOT Memory [Mb]
		541,3	
		2706,5	
237,2			0,3804
1186			1,902
	143,2		
	716		
		607,3	
		3036,5	
276,4			0,4766
1382			2,383
	200,2		
	1001		

Figure 8.5: Minimum Requirements

The values of $ROM = 1.4\ Mb$, $RAM = 3.8\ Mb$ and $throughput = 3.04\ MIPS$, which includes a 400% margin, has been evaluated as the minimum requirements for the On-Board processor. The On-Board microprocessor "MA31750" (a MIL-STD- 1750 based processor) [82] reaches a total value of memory of 16 *Mb* and a performance range of 0.7 up to 3.4 *MIPS* and it satisfies all the required performances. The real configuration has been also supported by two redundant memory modules of 224 Kwords that could help the system in peculiar request peak moments.

Bibliography

[1] . EUMETSAT, Metop-A URL: https://www.eumetsat.int/metop

[2] : EUMETSAT Annual Report 2017, https://web.archive.org/web/20181108025657/https://www.eumetsat.int/website/wcm/idc/idcplg?IdcService=GET_FILE&dDocName=PDF_AR_2017_EN&RevisionSelectionMethod=LatestReleased&Rendition=Web

[3] : Krebs, Gunter. https://space.skyrocket.de/doc_sdat/noaa-n.htm. Gunter's Space Page. Retrieved 27 December 2020.

[4] : eoPortal powered by ESA, MetOp (Meteorological Operational Satellite Program of Europe) URL: https://www.eoportal.org/satellite-missions/metop#gome-2-global-ozone-monitoring-expe

[5] : OSCAR, Observing Systems Capability Analysis and Review Tool URL: https://space.oscar.wmo.int/satellites/view/metop_a

[6] : EUMETSAT, Microwave Humidity Sounder MHS URL: https://www.eumetsat.int/mhs

[7] : EUMETSAT, Advanced Very High Resolution Radiomete AVHRR URL: https://www.eumetsat.int/avhrr

[8] : EUMETSAT, Advanced Data Collection System A-DCS URL: https://www.eumetsat.int/a-dcs

[9] : EUMETSAT, Search Rescue Processor and Repeater S&R URL: https://www.eumetsat.int/sarsat

[10] : EUMETSAT, Space Environmental Monitor SEM-2 URL: https://www.eumetsat.int/sem-2

[11] : EUMETSAT, Advanced Microwave Sounding Unit-A AMSU-A URL: https://www.eumetsat.int/amsu-a

[12] : EUMETSAT, Global Ozone Monitoring Experiment–2 GOME-2 URL: https://www.eumetsat.int/gome-2

[13] : EUMETSAT, GNSS (Global Navigation Satellite System) Receiver for Atmospheric Sounding (GRAS) URL: https://www.eumetsat.int/gnss-gras

[14] : EUMETSAT, Advanced SCATterometer ASCAT URL: https://www.eumetsat.int/ascat

[15] : EUMETSAT, High-resolution Infrared Radiation Sounder HIRS/4 URL: https://www.eumetsat.int/hirs

[16] : EUMETSAT, Infrared Atmospheric Sounding Interferometer IASI URL: https://www.eumetsat.int/iasi

[17] : ESA / Science Exploration / Human and Robotic Exploration / Mission Odissea - F. De Winne, "Baikonur: from the steppes of Kazakhstan to space",

[18] : François Spoto, Yves Bordes, Simon Chalkley, Luis Huertas Omar Sy MetOp Project Division, Projects Department, Directorate of Earth Obs ervations Programmes, ESTEC, Noordwijk, The Netherlands, " Preparing MetOp for Work"

[19] : K. Merz, M. A. Martín Serrano, D. Kuijper, M.A. García Matatoros, "The Metop-A Orbit acquisition strategy and its LEOP operational experience"

[20] : Francisco Sancho , David Lázaro , Pier Luigi Righetti, "out-of-plane manoeuvre campaigns for metop-a: planning, modelling, calibration and reconstruction, GMV at EUMETSAT, Eumetsat-Allee 1, D-64295 Darmstadt, Germany, Space Operations Consulting at EUMETSAT, Eumetsat-Allee 1, D-64295 Darmstadt, Germany, EUMETSAT, Eumetsat-Allee 1, D-64295 Darmstadt, Germany

[21] : EUMETSAT, "Goodbye, Metop A", URL: https://www.youtube.com/watch?v=GlijR58cSxc

[22] : Christelle Crozat, Pier-Luigi Righetti, Lionel de la Taille and Frank Perlik, Peter Collins, "MetOp-A Attitude and Orbit Control Operations", Telespazio at Eumetsat, Darmstadt, D-64293, Germany, Eumetsat, Darmstadt, D-64293, Germany, Vega at Eumetsat, Darmstadt, D-64293, Germany

[23] : Pier Luigi Righetti, Hilda Meixner, Francisco Sancho, Antimo Damiano, David Lazaro, "FLIGHT DYNAMICS PERFORMANCES OF THE METOP A SATELLITE DURING THE FIRST MONTHS OF OPERATIONS", Am Kavalleriesand 31, Darmstadt, D-64295, Germany

[24] : Francisco Sancho , David Lázaro , Pier Luigi Righetti, "out-of-plane manoeuvre campaigns for metop-a: planning, modelling, calibration and reconstruction, GMV at EUMETSAT, Eumetsat-Allee 1, D-64295 Darmstadt, Germany, Space Operations Consulting at EUMETSAT, Eumetsat-Allee 1, D-64295 Darmstadt, Germany, EUMETSAT, Eumetsat-Allee 1, D-64295 Darmstadt, Germany

[25] : Mirko Trisolini (1), Hugh G. Lewis (1), Camilla Colombo (2), "ON THE DEMISABILITY AND SURVIVABILITY OF MODERN SPACECRAFT", (1) Astronautics Research Group, University of Southampton, Southampton , SO17 1BJ, United Kingdom, (2) Department of Aerospace Science and Technology, Politecnico di Milano, Via La Masa 34, 20133, Milan, Italy

[26] : Ariane Group, 20N Chemical Monopropellant Thruster : https://www.space-propulsion.com/brochures/hydrazine-thrusters/hydrazine-thrusters.pdf

[27] : Eoportal powered by ESA, MetOp (Meteorological Operational Satellite Program of Europe): https://www.eoportal.org/satellite-missions/metop

[28] : Pierluigi Righetti, Jose Maria de Juana Gamo and Richard Dyer, "Mission Analysis of METOP-A End-of-Life Operation", EUMETSAT Allee, D-64295 Darmstad

[29] : ESA blog powered by ESA, EO Launch Campaing, METOP CHECKED FOR FUELLING, written by HONORA , From Nick (ESA), Baikonur, 24 April: https://blogs.esa.int/eolaunches/2012/04/24/metop-checked-for-fuelling/

[30] : K. Merz(1), M. A. Martín Serrano(2), D. Kuijper(3), M.A. García Matatoros(4), "THE METOP-A ORBIT ACQUISITION STRATEGY AND ITS LEOP OPERATIONAL EXPERIENCE", (1) EDS Operations Services at ESA/ESOC, Robert-Bosch-Strasse 5, 64293 Darmstadt, Germany, (2) SciSys Ltd at ESA/ESOC, Robert-Bosch-Strasse 5, 64293 Darmstadt, Germany, (3) LogicaCMG at ESA/ESOC, Robert-Bosch-Strasse 5, 64293 Darmstadt, Germany, (4) ESA/ESOC, Robert-Bosch-Strasse 5, 64293 Darmstadt, Germany

[31] : MT-Aerospace, PTD-96 Monopropellant Diaphragm Tank : https://www.mt-aerospace.de/files/mta/tankkatalog/PTD-96.pdf

[32] : SatCatalog, Propulsion sub-systems tanks catalogue : https://www.satcatalog.com/components/?subsystem=Propulsion+Subsystem&component-type=Tank&form-factor=SmallSat&vendor=&heritage=Yes&mass-min=0&mass-max=110.1&power-min=0&power-max=0.1&sort-by=None

[33] : Andrea Brandonisio, Michèle Lavagna, "Exercise Session: Propulsion System (PS)", 2023, Webeep-Politecnico di Milano.

[34] : Eoportal powered by ESA, MetOp (Meteorological Operational Satellite Program of Europe): https://www.eoportal.org/satellite-missions/metop

[35] : Andrea Brandonisio, Michèle Lavagna, "Telecommunication System (TMTC)", Politecnico Di Milano, A.A. 2022-2023.

[36] : Adam Farson, "What makes a good solid state-amplifiers?", VA7OJ/AB4OJ, may 2002. URL: https://www.ab4oj.com/quadra/sshfamp.html#:~:text=Adequate%20cooling%20and%20duty%20cycle%3A%20The%20efficiency%20of%20a%20solid,runs%20around%2045%20~%2050%25

[37] : Michèle Lavagna, "Preliminary Sizing & Margins Philosophy", Politecnico Di Milano, A.A. 2022-2023.

[38] : Marco Buemi, Jean-Michel Caujolle, Luis Huertas Martin, "MetOp-A satellite in orbit verification: The Challenge", EUMETSAT, Am Kavalleriesand 31 , 64295 Darmstadt, Germany, ESTEC, Keplerlaan 1, Postbus 299, 2200 AG Noordwijk, the Netherlands, 2008.

[39] : Finnish Transport and Communications AgencyFinnish Transport and Communications Agency, "RADIO FREQUENCY REGULATION" 7 November 2014.

[40] : Yunus Can Toy, Peyman Mahouti, Filiz Güneşì, Mehmet A. Belen, "Design and manufactering of an X-band horn antenna using 3-D printing technology", international conference on recent advances in space technologies 2017.

[41] : Scott H. Schaire, "Near Earth Network (NEN) Users' Guide", Goddard Space Flight Center.

[42] : Michael Gorbunov, ORCID, Vladimir Irisov,Christian Rocken, "Noise Floor and Signal-to-Noise Ratio of Radio Occultation Observations: A Cross-Mission Statistical Comparison", A. M. Obukhov Institute of Atmospheric Physics, Russian Academy of Sciences, Pyzhevsky Per. 3, 119017 Moscow, Russia, Spire Global, Inc., 1690 38th Street, Boulder, CO 80301, USA, Hydrometcenter of Russia, 13, Building 1, Bolshoy Predtechensky Lane, 123376 Moscow, Russia

[43] : Eoportal powered by ESA, MetOp (Meteorological Operational Satellite Program of Europe): https://www.eoportal.org/satellite-missions/metop

[44] : "Pointing budgeting using the ESA Pointing Error Engineering Handbook and Tool: benefits and limitations" Ott T., Wiedermann G., Crombez V., Damilano P. , Airbus Defence and Space, Germany. , Airbus Defence and Space, France. URL: http://peet.estec.esa.int/files/Pointing_Budgeting_ESAGNC2014.pdf

[45] : Francisco Sancho, Tatiana Paulino, José María de Juana, and Pier Luigi Righetti, "METOP-A DE-ORBITING USING VERY LARGE IN-PLANE MANEUVERS ",Darmstadt, Germany, URL:
https://issfd.org/2015/files/downloads/papers/117_Sancho.pdf

[46] : Francisco SANCHO, Jörg FISCHER, Stefania TARQUINI, "Non-nominal Attitude Manoeuvres during Metop-A extended Lifetime", Darmstadt, Germany, URL:
https://issfd.org/ISSFD_2017/paper/ISTS-2017-d-004__ISSFD-2017-004.pdf

[47] : "MetOp-A Attitude and Orbit Control Operations" Christelle Crozat, Telespazio at Eumetsat, Darmstadt, D-64293, Germany, and Pier-Luigi Righetti, Lionel de la Taille and Frank Perlik, Eumetsat, Darmstadt, D-64293, Germany, and Peter Collins, Vega at Eumetsat, Darmstadt, D-64293, Germany. URL: https://arc.aiaa.org/doi/pdf/10.2514/6.2008-3318

[48] : "Application of the attitude analysis of dynamics and disturbances tool in EUMETSAT study on thruster's allocation and momentum management for meteorological spacecrafts", Nuno Gomes Paulino, Stefano Pessina, Joao Branco, Thomas Peters.

[49] : "EUMETSAT STUDY FOR ATTITUDE DYNAMICS AND DISTURBANCES IN LEO AND GEO ENVIRONMENT", Pessina S., Gomes Paulino N.M.G., De Juana J.M., Righetti P..

[50] : "Attitude Determination and Control Systems", Scott R. Starin, NASA Goddard Space Flight Center John Eterno, Southwest Research Institute. 2010.

[51] : "CHEMICAL MONOPROPELLANT THRUSTER FAMILY ", 1N, 20N, 400N AND HERITAGE THRUSTER. ARIANEGROUP ORBITAL PROPULSION ROBERT-KOCH-STRASSE 1, 82024 TAUFKIRCHEN GERMANY.

[52] : "OUT-OF-PLANE MANOEUVRE CAMPAIGNS FOR METOP-A: PLANNING, MODELLING, CALIBRATION AND RECONSTRUCTION", Francisco Sancho, David Lázaro, Pier Luigi Righetti
https://issfd.org/ISSFD_2009/OperationsII/Sancho.pdf

[53] : "Attitude\orbit determination & Control, Michèle Roberta Lavagna, 2023, Webeep-Politecnico di Milano.

[54] : Eoportal powered by ESA, MetOp (Meteorological Operational Satellite Program of Europe): https://www.eoportal.org/satellite-missions/metop

[55] : "Improvement of the ESA-ESTEC large space simulator: Low temperature cooling loops installation and specific test equipment development for the METOP thermal vacuum tests", Gaetan Piret, Elena Checa, Silvio Dolce, Rene Messing, Roel Westara, ESA-ESTEC, Kepleraan, 1 2200AG Noordwijk, The Netherlands, URL: https://www.eoportal.org/satellite-missions/metop

[56] : Calvel, Bertrand, and Frederic Bernard. "IASI-NG development status." International Conference on Space Optics—ICSO 2018. Vol. 11180. SPIE, 2019.

[57] : Nasa Jet Propulsion Laboratory, California Institute of Technology
https://www.jpl.nasa.gov/images/pia18833-nasa-spacecraft-maps-earths-global-emissivit

[58] : Sheldal, "THE RED BOOk", , NORTHFIELD, MINNESOTA 55057 USA.
http://www.sheldahl.com/sites/default/files/Documents/ShieldingMaterials/RedBook.pdf

[59] : New Space Systems,
https://www.cubesatshop.com/wp-content/uploads/2016/06/NewSpace-Magnetorquer-Rod_7b.pdf

[60] :Spacecraft Sun Sensor, NATIONAL AERONAUTICS AND SPACE ADMINISTRATION, June 1970
https://ntrs.nasa.gov/api/citations/19710008281/downloads/19710008281.pdf

[61] CITAEL
http://www.sitael-hellas.com/wp-content/uploads/2015/10/Digital-Earth-Sensor.pdf

[62] : Pradeep Bhandari, "Robust Thermal Control of Propulsion Lines for Space Missions", Pasadena.

[63] : Ilaria Guarracino a, Alexander Mellor b, Nicholas J. Ekins-Daukes b, Christos N. Markides, "Dynamic coupled thermal-and-electrical modelling of sheet-and-tubehybrid photovoltaic/thermal (PVT) collectors", Clean Energy Processes (CEP) Laboratory, Department of Chemical Engineering, Imperial College London, South Kensington Campus, London SW7 2AZ, UK, Blackett Laboratory, Department of Physics, Imperial College London, South Kensington Campus, London SW7 2AZ, UK

[64] : Andrea Brandonisio, Michèle Lavagna, "Thermal Control System", Politecnico di Milano. A.A. 2022/2023.

[65] : Michèle Lavagna, "Thermal Control Sub-System", Politecnico di Milano. A.A. 2022/2023.

[66] : Eoportal powered by ESA, MetOp (Meteorological Operational Satellite Program of Europe): https://www.eoportal.org/satellite-missions/metop

[67] : ESA, Service Module electrical power, URL: https://www.esa.int/Applications/Observing_the_Earth/Meteorological_missions/MetOp/Electrical_power2

[68] : Calvel, Bertrand, and Frederic Bernard. "IASI-NG development status." International Conference on Space Optics—ICSO 2018. Vol. 11180. SPIE, 2019.

[69] : ESA, "Service Module electrical power", URL:
https://www.esa.int/Applications/Observing_the_Earth/Meteorological_missions/MetOp/Electrical_power2

[70] : ESA, "Spacecraft specifications", URL:
https://www.esa.int/Applications/Observing_the_Earth/Meteorological_missions/MetOp/Spacecraft_specifications

[71] : "REGULATED VS. UNREGULATED POWER SUPPLY", URL:
https://www.actpower.com/educational/difference-between-a-regulated-and-unregulated-p

[72] : "JS Davenport, MJH Chandler CEng, FIEE, FICE, FIHT, in Electrical Engineer's Reference Book (Sixteenth Edition), 2003", URL:
https://www.sciencedirect.com/topics/engineering/nickel-cadmium-battery#:~:text=Nickel%E2%80%93cadmium%20batteries,-Nickel%E2%80%93cadmium%20batteries&text=They%20operate%20over%20a%20wide,in%20various%20developmental%20electric%20vehicles

[73] : Michèle Lavagna, "Preliminary Sizing & Margins Philosophy", Politecnico Di Milano, A.A. 2022-2023.

[74] : Andrea Brandonisio, Prof. Michèle Lavagna, "Exercise Session: Electrical Power System (TCS)", POlitecnico Di Milano, 2022-2023

[75] . Soyuz to launch Metop-A, Starsem, URL: https://www.starsem.com/news/images/MetOp_launch_kit.pdf

[76] : Eoportal powered by ESA, MetOp (Meteorological Operational Satellite Program of Europe): https://www.eoportal.org/satellite-missions/metop

[77] : ESA, Service Module electrical power, URL: https://www.esa.int/Applications/Observing_the_Earth/Meteorological_missions/MetOp/Electrical_power2

[78] : EUMETSAT powered by ESA: URL: https://www.eumetsat.int/features/extending-working-lifetime-metop-weather-satellite

[79] : Pier Luigi Righetti, Richard Dyer, "Feasibility of Metop-A Mission Extension on Drifting Local Time", URL: https://issfd.org/ISSFD_2017/paper/ISTS-2017-d-001__ISSFD-2017-001.pdf

[80] : Wiley J. Larson, James Richard Wertz, "Space mission analysis and design", volume 3, Springer, 1992.

[81] : Andrea Brandonisio, Michèle Lavagna, "On-Board Data Handling System", 2022-2023

[82] : Datasheet catalog of MA31750: https://pdf.datasheetcatalog.com/datasheet/dynex/MA31750.pdf

[83] : Sutton, George P., and Oscar Biblarz. Rocket propulsion elements. John Wiley & Sons, 2016.